The Squeeze Film Damper over Four Decades of Investigations. Part I: Characteristics and Operating Features

L. Della Pietra and G. Adiletta

ABSTRACT—The present review aims to summarize the main research findings, in the last four decades, on the Squeeze Film Damper (SFD) and its application. In this first part, a survey of the construction characteristics and operating features of the SFD, as a separate component, is reported, as inferred from the technical literature consulted, through a number of theoretical approaches and experimental results. Part II of the paper will review research work on the dynamic behavior of rotors on supports equipped with SFDs.

KEYWORDS: Squeeze film dampers, dynamics of rotors, seals, fluid inertia effects, cavitation.

1. Introduction

This paper was conceived with the aim of summarizing the main results of research into the Squeeze Film Damper (SFD) and its application.

An SFD is a bearing assembly for supporting the shaft of high-speed rotors. It basically combines a bearing (generally a ball or roller, although different types of bearings, such as tilting-pad fluid bearings, can be adopted) and a damping oil film so as to determine a support provided with a suitable damping action. An illustration of this device is given in Figure 1. The shaft **P** of the rotor is supported by a roller bearing **J**, while an anti-rotation pin **T** prevents the outer race of the bearing from rotating. The *journal*, represented by the whole of **P** and **J**, is free to move in the fixed housing or *bearing* **B** that is integral to the frame **S**, thanks to a suitable radial clearance. The annulus is fed with lubricant, at a given pressure, that realizes the *squeeze film* **SF**. The precession motions of the journal, that is due to the residual unbalance of the rotor, cause a dynamic pressure distribution to originate in the squeezed oil film and consequent damping of the same motions can be obtained.

Besides being a widely used technical component for turbomachinery, the SFD has provided much material for research, because of its typical advantages and drawbacks, which are basically due to its nonlinear character. It was investigated by Cooper [1], about forty years ago, as a means to cut down the amplitude of rotor vibrations owing to unbalance. In the course of his investigation (a well known pioneering work into the present subject-matter, together with that of Friderícy et al. [2], according to the notes about the history of SFD development reported by Zeidan et al. [3]) Cooper experienced the benefits conferred on the rotor operation from the coupling of a damping element, represented by an oil squeeze film, to an elastic suspension placed within the rotor support (see Figure 2 and Part II of this review [4].)

This solution represented an improvement in the concept also investigated in those years regarding the opportunity of giving suitable flexibility to the supports, in order to obtain better performance for high-speed rotors [5]. However, the idea of combining the flexibility of the bearings for high-speed rotors with a consistent damping action arose well before, in addition to recourse to oil film as a means of damping the bearing vibrations. Some US patents of Birmann [6–8], issued from 1933 to 1948, are worthy of interest in this regard and a sort of SFD progenitor can be recognized in the devices (a number of concentric sleeves separated by capillary annuli filled with lubricant) equipping the turbine bearings shown.

Whether the SFD is adopted at the design stage or subsequently, as a retrofit component, its main advantages lie in the capability of reducing the effects of unbalance, i.e. the amplitude of rotor vibrations at resonance and the level of

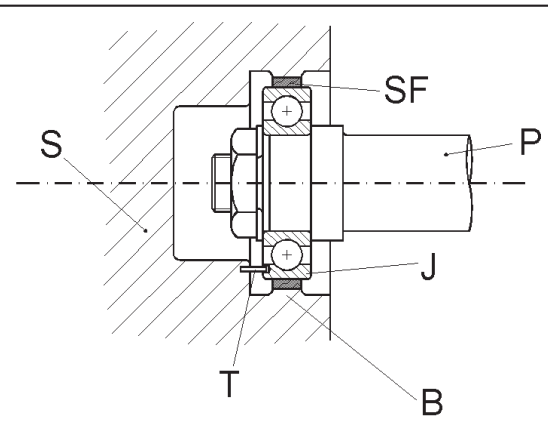

Figure 1. Draft of an SFD: **B** housing, **J** roller bearing, **P** journal of the rotor, **S** frame, **SF** squeeze film, **T** anti-rotation pin

Dipartimento di Ingegneria Meccanica per l'Energetica, Università degli Studi "Federico II", Napoli, Italy

The Shock and Vibration Digest, Vol. 34, No. 1, January 2002 3-26
©2002 Sage Publications

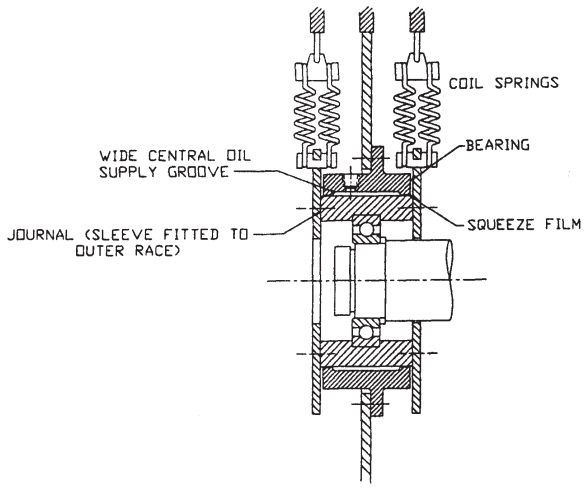

Figure 2. Draft of the Cooper's SFD (Courtesy of the Turbomachinery Laboratory [3])

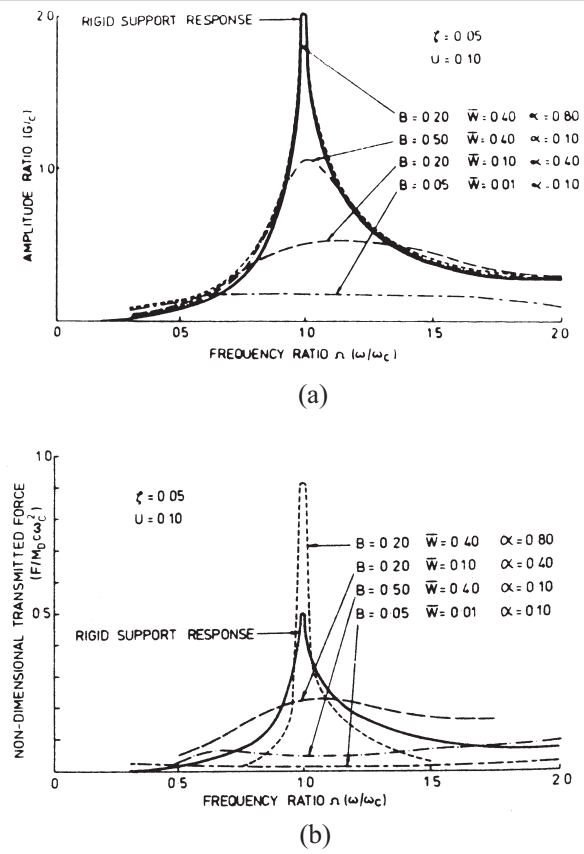

Figure 3. Comparison of the theoretical responses of an unbalanced flexible rotor, on rigid supports and SFD supports. (a) *vibration amplitude at mid-span* vs. *dimensionless speed*, (b) *transmitted forces at supports* vs. *dimensionless speed*. B, $\overline{W}$, and α are operating parameters relative to the operation with SFD supports (reproduced by permission of the ASME [15])

forces transmitted at supports under normal operating conditions, and in preventing the occurrence of non-synchronous instabilities or limiting their effects [9–14].

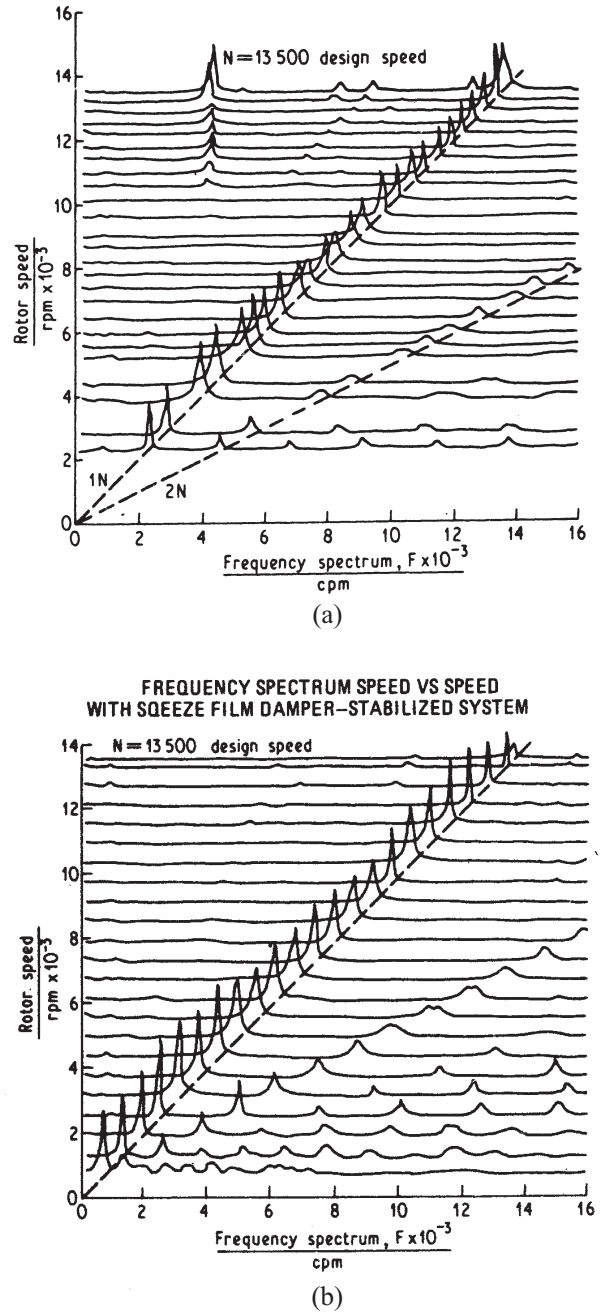

Figure 4. Example of suppression of the self-excited non-synchronous component relative to the operation of a centrifugal-compressor in tilting pad bearings. (a) *experimental frequency spectra* vs. *speed*, in the absence of SFDs, (b) case with SFD-mount of the supports (this material has been reproduced from [16] by permission of the Council of the Institution of Mechanical Engineers)

Figures 3 and 4 illustrate such favorable characteristics. The theoretical curves in Figures 3(a), (b) [15] represent the responses obtained with a model of unbalanced flexible rotor equipped with supports that were assumed rigid (i.e. devoid of SFD) in one case and mounted with SFD in other cases. In particular, operations with different arrangements for the SFD solution were respectively represented by different sets of the theoretical parameters assumed for the

model (B, $\overline{W}$ and α in the figure). The curves in Figure 3(a) show the predicted amplitude of vibration at rotor mid-span (amplitude ratio) versus the dimensionless rotor speed (frequency ratio). The pronounced peak at resonance obtained with rigid supports *is reduced or completely suppressed* with the adoption of SFDs. The predicted force transmitted at supports versus the dimensionless rotor speed is indicated in Figure 3(b). In this case too the presence of the SFD has an appreciable effect. *A marked reduction of the force transmitted at supports at resonance can be obtained, but it is also evident that this beneficial result is not assured whatever the set of parameters that characterize the SFD solution*. In particular, the curves show that in one case the level of force at resonance, in the presence of SFD, proves almost twice the corresponding level obtained with rigid supports.

The data reported in Figure 4, measured during the experimental test of a centrifugal compressor [16], highlight the capability of SFD in suppressing non-synchronous instabilities. The waterfall-plots in Figure 4(a) represent the frequency spectra of the vibration at a support of the rotor, in the absence of SFD, measured at different operating speeds along a run-up to 13,500 r.p.m. The main sequence of peaks, gathered along an oblique line, represents the synchronous component. A minor sequence of peaks, in vertical sequence within the plot (top), represents the non-synchronous vibration that occurs above 10,000 r.p.m. Figure 4(b) reports analogous data obtained in the presence of SFD. The suppression of the non-synchronous component is evident.

Since Cooper's investigation, the adoption of the SFD for turbomachinery has increased, extending its application from the original field of aircraft turbine engines to industrial process compressors and automotive turbochargers [3, 17, 18].

In the meantime, besides gaining greater insight into the features of this component, with attention paid particularly to the role of lubricant inertia, cavitation, sealing and feeding-geometry effects, research work has been addressed to experimenting improved solutions, aimed at improving SFD performance. The improvement was intended to overcome the typical drawbacks that can affect rotor operation in the presence of SFDs and optimizing some design aspects such as those connected to the compactedness of the rotor supports equipped with SFDs. In this respect, further developments are represented, on the one hand, by dampers that combine the traditional *passive* character of the conventional SFD with better efficiency and renewed design [19–21]. On the other hand, conceptual improvements are shown by solutions that adopt *active* control techniques for vibration reduction [22, 23] (a survey of the most recent developments is presented in Section 4 of Part II [4]).

In this respect, a brief review of theoretical and experimental analyses, regarding both the operating features of the SFD and the dynamic behavior of rotor-support systems incorporating SFDs, makes it possible to take stock of state-of-the-art research, after approximately four decades of investigations in this area. Further, the same review represents a short *excursus* through a significant chapter of rotordynamics where concepts and methods from nonlinear dynamics have played a major role.

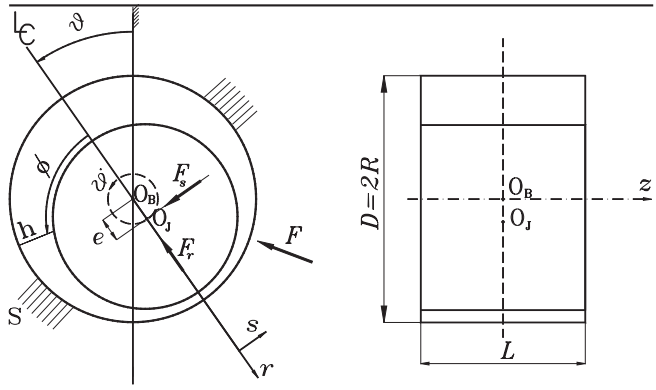

Figure 5. Scheme of the SFD and dynamic action originating during operation. Symbols: L axial length, D diameter, R radius, O_J journal center, O_B bearing center, e eccentricity, ϕ circumferential coordinate, ϑ attitude angle, $\boldsymbol{F}$ lubricant action onto the journal, $\boldsymbol{F}_r$, $\boldsymbol{F}_s$ radial and tangential components of $\boldsymbol{F}$, h local thickness of the annulus

For the sake of convenience, the general aspects and the investigations of the characteristics of the SFD, as a separate component, are dealt with in the present part of the review. An approach shared by a number of theoretical and experimental investigations, referred to below, consisted of *the analysis of the pressure distribution in the oil-film, the film forces, the influence of the boundary conditions connected to the supply and sealing, etc., carried out after assigning a relative motion to the members of the damper*. Different types of *controlled-orbit test rigs* were adopted, as a recurrent laboratory procedure, in order to put this sort of approach into practice. The survey presented in [4], instead, collected a number of studies where the SFD was investigated *within the ambit of rotordynamic evaluation*. These theoretical and experimental analyses were generally aimed to characterize the contribution of the damper to system behavior. Thus, *the motion* of well-balanced or unbalanced rotors, fitted with SFD-supports, and *the forces transmitted* through the SFDs, represented the *system response* generally analyzed with a view to *evaluating damper performance*.

2. General Aspects

In addition to Figure 1, a basic scheme for analyzing the damper is given in Figure 5, where the radial clearance C, i.e. the difference between the radius of the bearing and that of the journal, was intentionally exaggerated (the ratio R/C normally ranges in the interval $200 \div 1000$). The resulting pressure force $\boldsymbol{F}$ on the journal can be seen as the vectorial sum of a radial component $\boldsymbol{F}_r$ and a tangential force $\boldsymbol{F}_s$. The modulus F of $\boldsymbol{F}$ is a nonlinear function of the position and velocity of the journal.

A opposite force to $\boldsymbol{F}$ is transmitted to the frame of the machine. If the rotor is affected by static unbalance and Mu is the unbalance referred to the support, F is generally different from $Mu\omega^2$, the force transmitted in case of rigid support and shaft, i.e. when the outer race of the roller bearing is integral to the frame, in the absence of SF. The ratio

$$T = F / Mu\omega^2 \tag{1}$$

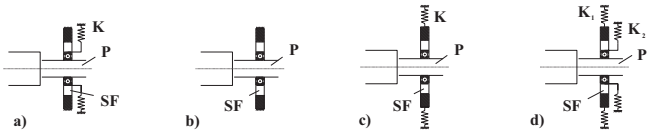

Figure 6. (a) Arrangement with centering springs parallel to the SF, (b) arrangement without elastic suspension, (c)-(d) schemes with additional stiffness in series to the SF. Symbols: K, K_1, K_2 retaining springs, P rotor journal, SF squeeze film

is indicated as the *transmissibility ratio*. For the SFD to work efficiently *T must always be less than 1 and the amplitude of the rotor motions must not be too large*.

When the rotor is at rest, no dynamic pressure originates in the oil film and the SFD has no static stiffness. As a consequence, in normal applications with horizontal rotors, the journal is at the bottom within the damper and only the increase in the rotor speed, subsequent to start-up, makes the same journal lift off, with parallel onset of the whirling motion of the rotor.

A suitable degree of stiffness may be introduced by means of a set of retaining springs, mounted parallel to the squeeze film (Figure 6(a)). In this case, the overall action transmitted to the frame of the machine is due to the squeeze film force $\boldsymbol{F}$ and the reaction of the elastic suspension. The addition of an elastic suspension to the SFD in the rotor supports allows some useful *tuning* of the rotor resonant frequencies, in order to assign a convenient range for the operating speeds [11, 24]. Furthermore, when the rotor is arranged horizontally and is at rest, a suitable preloading of the suspension makes it possible to center the journal with respect to the clearance. This way, precession motions, with trajectories of the journal that are *circular* and *centered* with respect to the bearing, can be reasonably assumed for *normal* operating conditions (i.e. *design* operating conditions) of the rotor, in the presence of acceptable levels of unbalance. The importance of realizing such *normal* conditions for the operation of the rotor and the role played by the centering suspension with regard to possible dynamic responses, including *jump phenomena* and *non-synchronous* motions, will be given particular attention in [4].

The most common arrangements for retaining springs are realized with the adoption of a *squirrel cage* bearing support (or a set of cantilever rods connected at one end to the outer race of the roller bearing) that requires a relatively large axial space in comparison to the damper length (Figure 7 [25]). This solution has been frequently adopted, for instance, in gas turbines for aeronautical engines. Sometimes, as in many applications for industrial lightweight compressors, a pair of elastomer O-rings in radial disposition (Section 4.3 and Figure 8(d)) can give the damping device some degree of stiffness, together with a sealing action, a contribution to damping and a partial compensation of eccentricity, at a modest expense of space, both in radial and axial directions (examples, with combination of SF and bearings of tilt pad type are given in [26, 27]). In this regard, it is also worth pointing out that, on the one hand, O-rings are widely adopted within damper bearings as seals and below, in Section 4.3, an illustration of typical schemes of mounting is given. On the other hand, in some

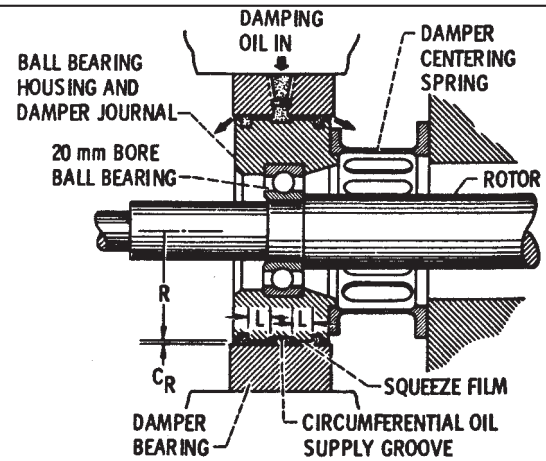

Figure 7. Illustration of a laboratory arrangement of SFD with centering spring of squirrel cage type (reproduced by permission of the ASME [25])

applications [28] the damping action of O-rings has justified their adoption within bearing assemblies as the only damping element, as an alternative to oil squeeze film (the dynamic characteristics of O-ring elastomeric dampers have been investigated by Smalley et al. [29]. Other arrangements for elastomeric dampers have been proposed in [30–32]).

However, the absence of centralizing suspension (Figure 6(b)) makes the actual realization of the support more straightforward than in the previous solution, even though not all the features of the parallel mounting of springs can be implemented and a more pronounced nonlinear behavior of the device can result. Some researchers go so far as to suggest the need for accurate design in order to maintain an adequate level of efficiency during operation [15]. As a matter of fact, the application of SFD in this simple configuration is normally restricted to the turbines for small aero engines or lightweight rotors for industrial compressors or automotive turbochargers, where space-saving is a lead criterion for manufacture, and the limited weight of the rotor makes it possible that the damper operates at its greatest efficiency.

Interestingly, further stiffness, with respect to the schemes of Figures 6(a)-(b), is introduced in the theoretical models, as illustrated in Figures 6(c)-(d), when the flexibility of the housing (*flexible housing effect*) is to be taken into account. An example of experimental arrangement where the flexibility of the housing was realized by means of flexible bars was given in [33] (see also Section 3.5 of Part II [4]).

White illustrated the outstanding aspects related to the dynamic behavior of a rotor supported with SFDs in his PhD thesis [34]. Even for the simple case of a rotor operating with a vertical axis and performing circular, centered whirl motions, White's theoretical analysis nevertheless pointed out that the dynamic behavior depends on the value of the dimensionless unbalance and that *multi-stable* operating conditions, with *jump-up* or *jump-down*, may arise as a result of the nonlinearity of the oil film forces. White furthermore gave experimental proof of the fact that the dynamic behavior of the rotor was qualitatively in agreement with the theoretical predictions, even though the effective response of the squeeze film could turn out to be quite

different from the theoretical one, depending on some factors among which he highlighted the possible presence of rupture in the film and the actual size of the cavitated zone.

The above aspects and other ones like fluid inertia effects, the geometry of grooves for the oil supply and drain, the presence of seals, etc., have addressed a considerable part of the research work into characterization of the SFD response, from both a theoretical and an experimental point of view.

3. The Hydrodynamic Forces in an SFD

The precession motions of the journal of the SFD give rise to a pressure distribution within the film that can be determined with the theory of hydrodynamic lubrication, through which the viscous and inertial nature of the hydrodynamic action, associated to the squeeze action, are taken into account. The resultant of the forces acting on the journal is obtained by means of integration of the pressure distribution in the film. In this regard some aspects must be noted:

- The pressure distribution can be expressed analytically on condition that suitable hypotheses are given. Otherwise, it is to be determined with recourse to numerical integration of partial differential pressure equations.
- The integration of the pressure distribution depends on how the cavitated zones are treated, where the pressure in the film turns out to be non-positive. During operation, cavitation can be manifested in different ways (see Section 6 and Part II) that govern the aspect of the cavitated zone and the pressure therein, mainly depending on the journal motion, the level and geometry adopted for oil supply, and the presence of seals. It should be observed that the value of the pressure of cavitation p_c cannot be given univocally. Most researchers set p_c equal to ambient pressure. Laboratory tests have shown p_c values to be equal to the *ambient pressure*, to the *vapor pressure*, or to *negative absolute pressures* (see Section 6 and Part II). A straightforward and broadly adopted approach, in order to carry out the integration of pressure distribution, consists in curtailing the pressure contribution within the cavitated zone, where a null relative pressure is assumed, regardless of proper conditions for the pressure gradients along the boundary of the cavitated region.
- Once the contribution of the cavitated region to the pressure force is excluded, the scalar components of the film force on the journal F_r and F_s, respectively taken along the radial and tangential directions (refer to the notation in Figure 5 and assume the axial co-ordinate $\zeta = z/L$), are expressed as

$$F_r = LR\int_{-\frac{1}{2}}^{\frac{1}{2}}\int_{\phi_1}^{\phi_2} p\cos\phi \; d\phi \; d\zeta$$

$$F_s = LR\int_{-\frac{1}{2}}^{\frac{1}{2}}\int_{\phi_1}^{\phi_2} p\sin\phi \; d\phi \; d\zeta \qquad (2)$$

  where the angular limits ϕ_1 and ϕ_2, depending on the effective extension of the cavitated zone, can vary along the circumferential and axial directions.
- With regard to the expression of the radial and tangential components of the pressure force, F_r and F_s, those types of journal motions that represent *normal* operating conditions of a rotor merit particular interest. In particular, precession motions with the journal center covering trajectories that are *approximately circular and centered* with respect to the bearing (the acronym CCO is used for *circular centered orbits*) can be assumed for the SFD with centering elements. When the elastic suspension system is absent or does not achieve a complete initial centering of the rotor at rest, *normal* operation represented by orbits *about an off-center position* is taken into account. Expressions of the film force components by means of *force coefficients* prove particularly suitable for rotor-dynamic analyses that refer to such conditions of motion.

With the adoption of polar co-ordinates e and ϑ for expressing the position of the journal center O_J (Figure 5), F_r and F_s are given in the most general case [35] by

$$F_r = -C_{rr}\dot{e} - C_{rs}e\dot{\vartheta} - M_{r\,\mathrm{rad}}\ddot{e} - M_{r\,\mathrm{non}}\frac{\dot{e}^2}{e} - M_{r\,\mathrm{tan}}e\ddot{\vartheta} - M_{r\,\mathrm{cor}}2\dot{e}\dot{\vartheta} + M_{r\,\mathrm{cen}}e\dot{\vartheta}^2$$

$$F_s = -C_{sr}\dot{e} - C_{ss}e\dot{\vartheta} - M_{s\,\mathrm{rad}}\ddot{e} - M_{s\,\mathrm{non}}\frac{\dot{e}^2}{e} - M_{s\,\mathrm{tan}}e\ddot{\vartheta} - M_{s\,\mathrm{cor}}2\dot{e}\dot{\vartheta} - M_{s\,\mathrm{cen}}e\dot{\vartheta}^2. \qquad (3)$$

In the above expressions, the nonlinear terms with $\dot{e}^2/e$ appear in addition to those representing the radial, tangential and Coriolis acceleration of the journal center. The coefficients C_{ij} and M_{ij} represent force factors that are distinctive of the *damping* and *inertia* contributions, respectively.

In dimensionless form, expression (3) can be written as [36]:

$$\overline{F}_r = -\overline{C}_{rr}\varepsilon' - \overline{C}_{rs}\varepsilon\vartheta' - \mathrm{Re}^*\left(\overline{M}_{r\,\mathrm{rad}}\varepsilon'' + \overline{M}_{r\,\mathrm{non}}\frac{\varepsilon'^2}{\varepsilon} + \overline{M}_{r\,\mathrm{tan}}\varepsilon\vartheta'' + \overline{M}_{r\,\mathrm{cor}}2\varepsilon'\vartheta' - \overline{M}_{r\,\mathrm{cen}}\varepsilon\vartheta'^2\right)$$

$$\overline{F}_s = -\overline{C}_{sr}\varepsilon' - \overline{C}_{ss}\varepsilon\vartheta' - \mathrm{Re}^*\left(\overline{M}_{s\,\mathrm{rad}}\varepsilon'' + \overline{M}_{s\,\mathrm{non}}\frac{\varepsilon'^2}{\varepsilon} + \overline{M}_{s\,\mathrm{tan}}\varepsilon\vartheta'' + \overline{M}_{s\,\mathrm{cor}}2\varepsilon'\vartheta' + \overline{M}_{s\,\mathrm{cen}}\varepsilon\vartheta'^2\right) \qquad (4)$$

with $\varepsilon = e/C$: dimensionless eccentricity, Re*: modified Reynolds number of the SFD (see below in this section), ', " : derivatives with respect to dimensionless time $\tau = \omega t$ (t dimensional time, ω reference value for the angular frequency of the journal precession), and the dimensionless coefficients $\overline{C}_{ij}$ and $\overline{M}_{ij}$ can be expressed as a function of the respective dimensional coefficients C_{ij} and M_{ij} as will be shown below.

Re* is the *modified Reynolds number* (or *squeeze film Reynolds number*, sometimes *gap Reynolds number*) defined as

$$\mathrm{Re}^* = C^2\omega / \nu \qquad (5)$$

where ω and ν represent the angular frequency of the journal precession and the kinematic viscosity of lubricant,

respectively. The forces that are due to the fluid inertia can be neglected for Re* < 1 [37, 38].

The components of the force can also be expressed in a fixed Cartesian reference frame. It is worth noting that the coefficients in expression (4) stem from integration, in accordance with (2), and can be given an analytical aspect, under suitable hypotheses, as will be reported below.

With regard to the use of force coefficients, when a steady-state equilibrium position of the journal (static or dynamic equilibrium conditions, respectively represented, for instance, by a generic, static, off-center position or by a steady-state circular centered orbit) can be assumed as a reference, a linearization of the film force can be given in the neighborhood of the said reference position. Thus *linearized stiffness, damping* and *inertia coefficients* can be obtained through a *perturbation* of the steady-state condition, corresponding to partial derivatives of the components of the film force. With reference to the motion of a rotor, these coefficients are adopted in analyses of the linear stability of the equilibrium motion (see [34, 39], as examples, and Part II) or when the same motion is to be sought by means of perturbation methods ([40] and Part II).

Early investigations to evaluate the hydrodynamic action in SFDs were based on the ordinary hypotheses of the lubrication theory for isoviscous, incompressible fluid and laminar flow. The role of the fluid film inertia was subsequently recognized and theoretical and experimental analyses were addressed to this subject. Since the SFD can operate in conditions characterized by negligible inertia effects in the fluid film, the results related to the analysis of SFD characteristics in the absence of fluid inertia will be reported first, followed by those regarding the studies where the role of inertia was taken into account.

4. Hydrodynamic Forces in the Absence of Inertia

This section provides the differential equations that govern the pressure distribution in the fluid film. The law of the pressure and expressions of F_r and F_s components are reported with relation to the cases in which the above differential equations can be analytically integrated. These equations hold under the hypotheses of laminar, isoviscous lubricant flow and no inertia effects. It must be observed that the laminar flow hypothesis was shared by almost all the consulted papers. According to Tichy [38], the transition to turbulent conditions would arise with the following values $\mathrm{Re}_{\mathrm{TR}}$ of the Reynolds number Re ($\mathrm{Re} = \rho\omega RC/\mu = \mathrm{Re}^* \cdot R/C$, with μ and ρ denoting the dynamic viscosity and the density of the fluid, respectively):

$$\mathrm{Re}_{\mathrm{TR}} = 5600 \text{ (low values of Re*)};$$

$$\mathrm{Re}_{\mathrm{TR}} = 1400\sqrt{\mathrm{Re}^*} = 1400 \text{ (high values of Re*)}.$$

4.1. The Reynolds Equation

With reference to Figure 5, the bidimensional Reynolds equation can be written:

$$\frac{\partial}{\partial\phi}\left(\bar{h}^3\frac{\partial\bar{p}}{\partial\phi}\right)+\left(\frac{R}{L}\right)^2\frac{\partial}{\partial\zeta}\left(\bar{h}^3\frac{\partial\bar{p}}{\partial\zeta}\right)=12\left(\vartheta'\varepsilon\sin\phi+\varepsilon'\cos\phi\right) \quad (6)$$

Where $\bar{p} = p/\left(\mu\omega R^2/C^2\right)$ is the dimensionless pressure and $\bar{h} = h/C$ the dimensionless thickness of fluid film. ϑ' denotes the angular frequency of precessional motion of the journal. ϑ' and ε' represent derivatives with respect to the dimensionless time (i.e. $\tau = \omega t$, with t and ω denoting the dimensional time and a reference angular speed or frequency, respectively). The solution of equation (6) can be sought using numerical procedures, once a suitable set of boundary conditions has been assigned, mostly depending on the way the oil is supplied to the film, the degree and type of sealing, and the possible presence of cavitation in the film. As is well known, analytical solutions are generally difficult or impossible to obtain, especially when realistic boundary conditions for the film are taken into account.

On the other hand, approximated expressions of the Reynolds equation allow straightforward closed-form solutions. For the *short bearing approximation* ($L/D \to 0 \Rightarrow \partial\bar{p}/\partial\phi << \partial\bar{p}/\partial z$), and the *long bearing approximation* ($L/D \to \infty \Rightarrow \partial\bar{p}/\partial z << \partial\bar{p}/\partial\phi$), respectively, equation (6) can be rewritten:

$$\frac{d}{d\zeta}\left(\bar{h}^3\frac{d\bar{p}}{d\zeta}\right)=12\frac{L^2}{R^2}\left(\vartheta'\varepsilon\sin\phi+\varepsilon'\cos\phi\right) \quad (7)$$

$$\frac{d}{d\phi}\left(\bar{h}^3\frac{d\bar{p}}{d\phi}\right)=12\left(\vartheta'\varepsilon\sin\phi+\varepsilon'\cos\phi\right). \quad (8)$$

Besides the above approximations, which are briefly outlined in the following section, it is also worth mentioning the *Warner approximation* (*WA*) for the analytical approximate characterization of *finite length* bearings. Thus the effective pressure distribution is obtained multiplying a LBA pressure profile by a suitable *end-leakage function* [39, 42] (for the case of small journal eccentricity see also [43]).

4.2. Analytical Expressions for Pressure Distribution

a) Short bearing approximation

The *short bearing approximation* (*SBA*) (aka *Ocvirk solution*), corresponding to the limit condition $L/D \to 0$, has been widely adopted in the investigations for dampers with no seals (open-ends) and $L/R < 0.5$. Double integration of (7) makes it possible to write:

$$\bar{p} = 6\frac{L^2}{\bar{h}^3R^2}\left(\vartheta'\varepsilon\sin\phi+\varepsilon'\cos\phi\right)\left(\zeta^2-\frac{1}{4}\right) + \left(\bar{p}_1-\bar{p}_2\right)\zeta+\frac{1}{2}\left(\bar{p}_1+\bar{p}_2\right) \quad (9)$$

where $\bar{p}_1$ and $\bar{p}_2$ are the values assigned to the dimensionless *absolute* pressure on both sides of the film ($\zeta = \pm 0.5$) in order to represent, for instance, different values of the supply pressure and discharge pressure, respectively. The given supply pressure can be related to the presence of a circumferential groove, with the assumption that the fluid film is fed along the whole circumference. In this circumstance, expression (9) can be assumed to be valid only when the oil inlet flow is adequate. In the presence of circular centered orbits (CCOs), with $\varepsilon' = 0$, $\vartheta' = 1$ and zero *relative* pressure on both sides of the bearing (i.e. $\bar{p}_{1\,\mathrm{rel}} = \bar{p}_{2\,\mathrm{rel}} = 0$), the following expression of the *relative*

pressure distribution can be given in the middle plane of the damped bearing, at $\zeta = 0$:

$$\bar{p}_{0\,\mathrm{rel}} = -\frac{3}{2}\left(\frac{L}{R}\right)^2 \frac{\varepsilon \sin\phi}{\left(1+\varepsilon\cos\phi\right)^3}. \tag{10}$$

A comparison between the numerical solution obtained for a damper of finite length and the analytical solution corresponding to the SBA was carried out in [34].

Expression (9) shows the dependence of the pressure distribution on the components of the journal velocity. El-Shafei and Eranki [44] reported the pressure profiles for different ratios of the radial velocity $\dot{e}$ to the tangential one $e\dot{\vartheta}$ (and zero relative pressure on both sides of the bearing). In all cases the region of relative positive pressure had circumferential extension of about π radians, even though its position changed from case to case. This result is an example that supports the broad use of π-film cavitation theory in combination with the SBA. However, the type of motion and trajectory has great influence in determining the actual position of the cavitated region and, consequently, the angular limits for integrating pressure distribution. This observation is to be kept in mind when the resultant film-force and the relative coefficients are expressed, as will be shown below, in closed form from (9)–(10). The validity of the obtained coefficients depends on the correct use of proper limits of integration that are consistent with the journal motion.

b) Long bearing approximation

When the Reynolds equation is simplified with the *long bearing approximation* (*LBA*) (aka *Sommerfeld solution*), corresponding to the limit condition $L/D \to \infty$, the pressure distribution is obtained by means of integration of equation (8) with the boundary conditions represented by assuming $\bar{p} = \bar{p}_0$ at the section of maximum clearance (i.e. at $\phi = 0$ and $\phi = 2\pi$):

$$\bar{p} = \bar{p}_0 - 12\,\vartheta'\left(\frac{\varepsilon}{2+\varepsilon^2}\right)\frac{\left(2+\varepsilon\cos\phi\right)\sin\phi}{\left(1+\varepsilon\cos\phi\right)^2} + 6\frac{\varepsilon'}{\varepsilon}\left(\frac{1}{\left(1+\varepsilon\cos\phi\right)^2} - \frac{1}{\left(1+\varepsilon\right)^2}\right) \tag{11}$$

If $\bar{p}_0$ is high enough, the pressure remains higher than the cavitating pressure anywhere, with no rupture of the film, and the net film-force on the journal merely depends on the pressure difference $\Delta\bar{p} = \bar{p} - \bar{p}_0$. By contrast, the pressure distribution (11) cannot actually be maintained at locations where the pressure proves lower that the pressure of cavitation $\bar{p}_c$. An example of a suitable expression of $\bar{p}_0$ that suits real cases is given in [45]. In the case of CCOs, with $\dot{\vartheta} = \omega$, $\vartheta' = 1$, the dimensionless pressure difference $\Delta\bar{p} = \bar{p} - \bar{p}_0$ is

$$\Delta\bar{p} = -\frac{24\varepsilon\sin\phi + 6\varepsilon^2\sin 2\phi}{\left(2+\varepsilon^2\right)\left(1+\varepsilon\cos\phi\right)^2}. \tag{12}$$

Instances of the pressure profiles obtained with different values of the dimensionless eccentricity and of the γ ratio between the radial and the tangential components of the journal velocity, i.e. $\gamma = \dot{e}/e\dot{\phi}$, were reported in [44]. Unlike the SBA cases, the data show an appreciable dependence of the circumferential extension of the cavitated region on the ratio in question. In particular, uncavitated conditions (i.e. 2π-film) can be approached with high ratios. By contrast, large negative ratios make the cavitated region much higher than π. On the other hand, the extent of the cavitated region and its position are independent of the journal eccentricity. These results further substantiate the observations made at the end of the previous section about the dependence of the film-force coefficients and their validity.

In [46, 47] the integration of (8) was carried out, assuming for the pressure a function with harmonic components in ϕ and 2ϕ and adopting the two continuity boundary conditions $\bar{p}(\phi = 0) = \bar{p}(\phi = 2\pi)$. The obtained distribution, indicated as *hydrodynamic pressure*, coincides with the expression of $\Delta\bar{p} = \bar{p} - \bar{p}_0$ obtained from (11) for null radial velocity. By contrast, the difference between the hydrodynamic pressure and $\Delta\bar{p}$ is a function of the dimensionless eccentricity and of the γ ratio between the radial and tangential components of the journal velocity:

$$\frac{-\gamma\,(\varepsilon+4)}{(2+\varepsilon^2)(1+\varepsilon^2)}.$$

Examples of the total pressure distributions resulting from superposition of the *hydrodynamic*, *inlet* and *cavitation* pressure are given in [46]. In [47] the theoretical pressure distributions for eccentric circular orbits were reported.

A comparison between (10) and (12) can be drawn after assuming $\bar{p}_0$ equal to zero *relative* pressure and shows that, for the L/R values usually adopted in SFD implementations ($L/D < 0.5$), the values attained by the circumferential pressure under the LBA (i.e. with $L/R \to \infty$) prove much higher than those obtained with the SBA.

The LBA is reasonably valid in the presence of seals for the film [46–48], with very small oil leakage, so as to make the pressure gradient in the axial direction negligible with respect to the circumferential gradient. Lund et al. [49] and Holmes and Dogan [33] pointed out that its validity also depends on oil supply. For instance, a circumferential groove in the middle plane of the bearing represents an unconstrained boundary condition for the oil film and is thus incompatible with the above hypothesis. However, a series of small feeding holes arranged around the circumference is more congruent with the long bearing model. On the other hand, the latter solution might entail the problem of a reverse flow through the inlet holes if the pressure in their neighborhood reaches high values, thus causing the oil supply to be insufficient and determining a dynamic response that differs from the predicted one. If the film is fed with a single hole, and the inlet is sufficiently unrestricted so that the pressure of the SF, at the inlet, can be assumed to remain at the supply pressure, the expression that predicts the pressure measured at a fixed circumferential location, by a pressure transducer for CCOs, was given in [48].

4.3. Boundary Conditions for the Seals

The use of seals in SFD mountings aims to increase the damping features by restricting or preventing the side leakage of the lubricant, though introducing some increase in

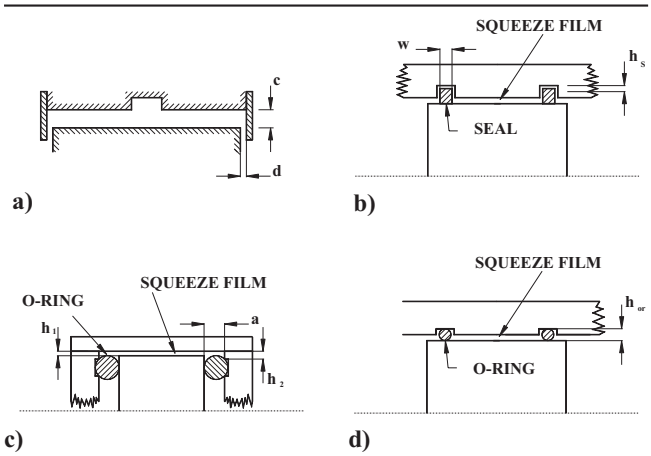

Figure 8. Different types of seal arrangements

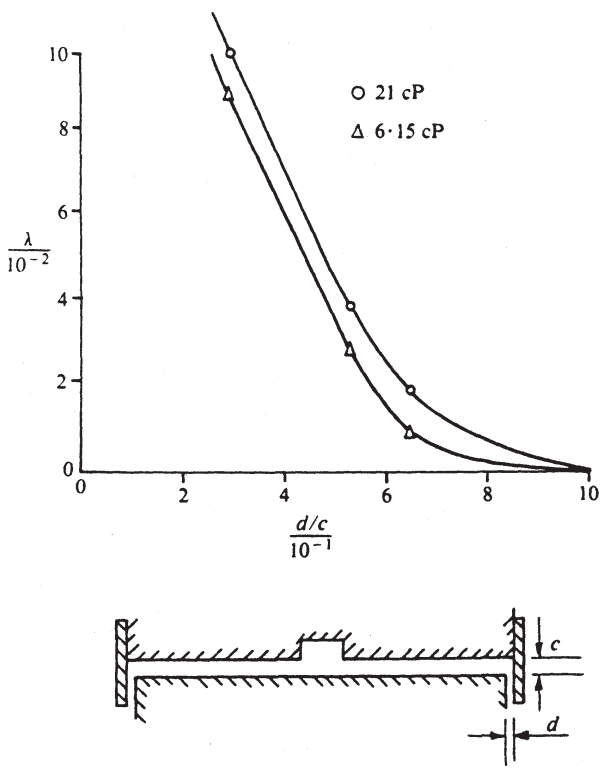

Figure 9. λ coefficient versus seal geometry parameter *d/c*, with two different values of lubricant viscosity (reproduced by permission of the ASME [45])

the fluid temperature and a consequent lowering of viscosity. The main seal schemes are shown in Figure 8 and were reported in [45, 50]. In particular, schemes 8(b) and 8(c) were indicated in [49] as *local seal* and *global seal*, respectively. With respect to the solution of the bidimensional Reynolds equation, the presence of seals imposes a set of boundary conditions, expressed by means of relationships that are consistent with the adopted seal arrangement, which can be generally dealt with within a numerical scheme.

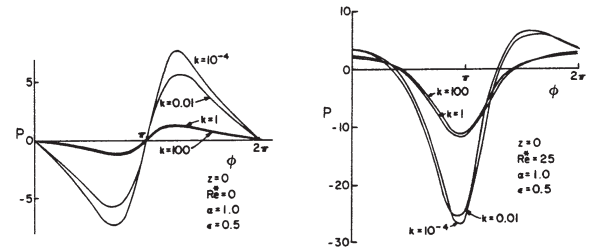

Figure 10. SFD pressure, with circular, centered orbits of the journal center and varying the seal performance (*k* coefficient): (a): with no fluid inertia effects; (b) with fluid inertia effects (reproduced by permission of the ASME [51])

The seal arrangement depicted in Figure 8(a) was indicated as a *small clearance seal* [50] and the following empirical law for the pressure distribution was suggested in [33, 45]:

$$p(\zeta,\phi) = p_{SH}(\zeta,\phi) + \lambda p_L(\phi). \tag{13}$$

In the above relation $p_{SH}(\zeta,\phi)$ and $p_L(\phi)$ are, respectively, the pressure distributions obtained under the SBA and LBA, and λ is a factor whose value is in the range (0, 1), depending on the characteristics of the seal.

After comparing the experimental results with the predicted data, Dede et al. [45] suggested the law illustrated in Figure 9 for λ. As can be observed, the value of λ depends not only on seal geometry but also on fluid viscosity.

An example of the boundary conditions for the above seal arrangement was also given in [51]. Some of the results illustrated therein, with regard to the seal effects on the pressure distribution, are show in Figure 10(a), (b). The *k* parameter is a leakage coefficient whose value decreases as seal efficiency increases. Figure 10(b) shows the effect of varying *k* in the presence of fluid inertia.

An example of analytical condition for the arrangement in Figure 8(b) (*piston ring seal*) was given in [50]. The condition establishes a *local* relationship at the boundary, between the axial pressure gradient and the pressure drop through the seal, caused by fluid passing from the damper to the external environment. A characteristic leakage coefficient appears in the condition, with a value that is in the range from 0 to 1. Tecza et al. [52] pointed out the uncertainty affecting the actual value of the pressure drop in the seal and, consequently, the value of the leakage coefficient on which the pressure law in the film depends. The magnitude of the pressure drop can be approximately determined using static tests. In [49] boundary conditions were expressed for seals whether or not provided with side groove, with use of a global outflow coefficient or a local coefficient, respectively. In [45] the empirical law (15) for the seal geometry of Figure 8(a) was discussed through a suitable comparison of the pressure distributions with those obtained with adoption of the boundary condition reported in [50] for the scheme of Figure 8(b).

In the case of Figure 8(c) the seal is represented by means of an O-ring placed laterally to the film (*side O-ring seal*), in a groove whose dimensions (a and h_2 in the figure) are somewhat greater than the thickness h_1 of the film. The boundary condition can be written by making a global balance of the axial flow through the film edge and the seal. In particular, since $h_2 >> h_1$, both the circumferential flow and

the related pressure gradient in the seal can be neglected. In [50] an expression of the boundary condition was given, with use of a global outflow coefficient condition whose value depends on the possible presence of drain holes and the element specifically adopted for the seal.

In the seal arrangement in Figure 8(d) (*radial O-ring seal*), the O-ring is deformed with the rotating pressure distribution so as to give rise to an axial flow, even in the absence of leakage from the seal. The analytical condition that expresses the balance of flow, *locally* given along the circumferential arc of the fluid film edge and function of a suitable outflow coefficient, can be found in [50].

Recourse to elastomeric seals, in particular, takes into account the possible influence of their inherent stiffness and damping capacity (hints in Section 2) on the whole dynamic behavior of the SFD. Nevertheless, only a limited number of papers, within the consulted literature, comment explicitly on the dynamic characteristics of the O-rings included in the damper assemblies analyzed [53–55]. Apart from particular operating conditions or mountings or applications, such as those mentioned in Section 2 (adoption of the O-ring within bearing assemblies principally as a damping and elastic element), the above aspects normally prove to be of minor importance with respect to those capable of exerting a significant influence on the hydrodynamics of the SFD operation. In this sense, a notable aspect connected to the presence of seals consists in the end leakage *vs* pressure drop relationship that allows accurate prediction of the SFD response [3]. This substantiates the importance of the boundary seal conditions examined earlier in this section (for instance, see also [56]). It is worth pointing out that whatever the type of seal adopted, in practice the actual damper performance can only be compared with the predicted one after making a preliminary experimental evaluation of the coefficients in the expressions given for the pressure drop [57]. Obviously, the above considerations cannot be generalized to other rotordynamic cases characterized by conditions (in the presence of different bearings or seals), with dynamic coefficients of the seals that are of the same order of magnitude as the bearing coefficients [26].

4.4. Boundary Conditions for Oil Inlet and Oil Outflow

When the oil is supplied to the damper by means of a groove over the whole circumferential edge of the film, the boundary condition is merely represented by (for instance [49]):

$$p_i = p_a \tag{14}$$

where p_i is the pressure value at the inlet edge of the fluid film and p_a is the supply pressure.

This hypothesis is generally not appropriate. On the one hand the pressure value in the groove may turn out to be very different from the supply value and, on the other, the geometry of the groove itself influences the behavior of the damper [13, 58, 59, 60 (p. 187), 61] in addition to other factors, such as lubricant inertia, turbulence effects and the possible presence of valves (check or needle valves) at the inlet and/or outlet [60 (pp. 206–210, pp. 229–230)].

For instance, Walton et al. [62] observed a noticeable reverse flow of lubricant, both axial and circumferential, with the rupture of the film. Dynamic pressures whose amplitudes in the supply groove were about 1/3 of those detected in the fluid film were observed by San Andrés [60 (p. 192)] and San Andrés and Vance [61] who expressed the pressure drop at the fluid film discontinuity through a suitable coefficient inferred by experimental results (see Section 6.2 for some experimental work related to the present section). Arauz and San Andrés [58] and San Andrés [63] investigated the influence of a feeding groove. In [63] it was inferred that, for small amplitude centered orbits of the journal center and low driving frequencies, the SFD with two lands and the central groove in the middle operated like an SFD with a single land, whose axial length was the sum of the two land lengths and the groove width. In [58], under the same hypothesis of small centered orbits, the pressure distribution was theoretically predicted with different dimensions assigned to the feeding groove, also taking into account the circumferential flow of lubricant into the same groove. Figure 11 (from [58]) illustrates the diagram of the dimensionless axial pressure in a single land of the damper, for different ratios of the groove depth *cg* to the radial clearance *c*.

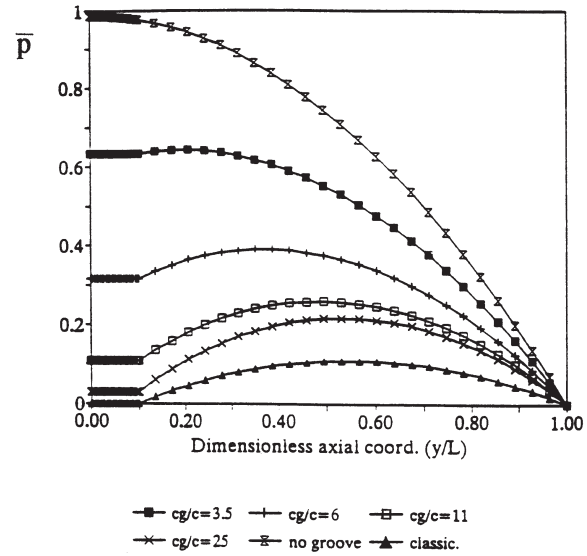

Figure 11. Axial pressure in the damper, varying the *cg/c* ratio (*cg*: depth of the groove), with fixed *Lg/L* ratio (*Lg*: axial length of the groove) (reproduced by permission of the ASME [58])

Even if the *cg/c* ratio was given the value of 25, the pressure attained values higher than those predicted by the simple theory. Figures 12(a)-(b) show the influence of the *cg/c* ratio on the amplitude of the radial and tangential force components, for an assigned *Lg/L* ratio (*Lg*: length of the groove). In this respect, it can be inferred that the presence of a central groove can give the damper more efficiency in relation to the predictions of the simple theory, obtained under the boundary condition (14).

On the other hand, the damping performance of the fluid film can be increased by supplying the lubricant to the film either by means of a suitable number (two or four) of inlet holes, instead of the groove in the middle plane of the damper, or by means of a pair of suitably sealed grooves placed at either end of the film [64].

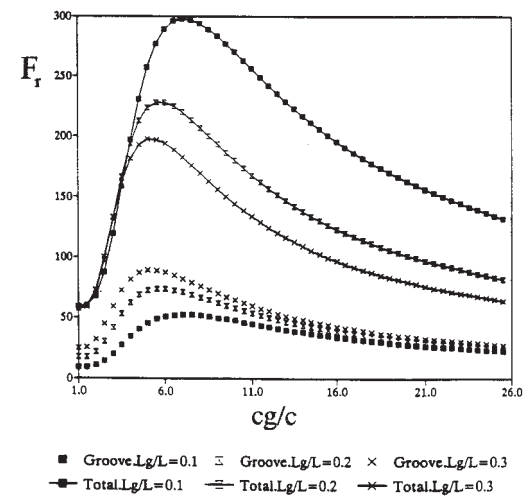

(a)

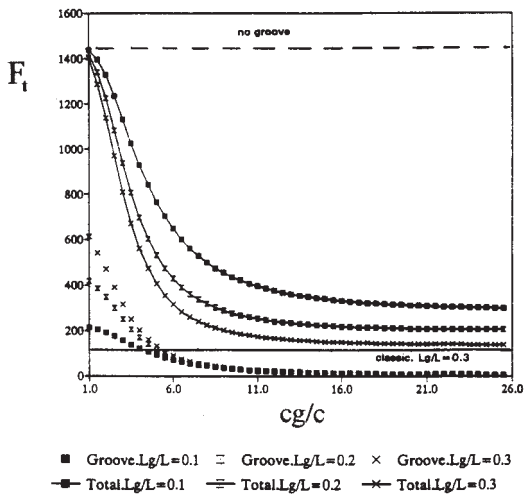

(b)

Figure 12. Squeeze film force components varying the *cg*/*c* ratio (*cg*: depth of the groove), with different *Lg*/*L* ratios (*Lg*: axial length of the groove) and assigned *e*/*c* ratio: (a) radial component; (b) tangential component (Reproduced by permission of the ASME [58])

The solution that makes use of inlet holes can also be affected by temporary inversion of lubricant flow in the feed holes [49, 62]. In [49] the condition adopted for expressing the pressure at a generic inlet hole was given: $p_f = p_{sf} - \alpha_f\, q_f$, where p_{sf} and q_f are the supply pressure (usually the pressure in the annular chamber connected to the inlet holes) and the flow at the given hole; α_f is a coefficient expressing the pressure drop through the hole.

In [50] the boundary condition for a single inlet hole with backflow was given by equating the flow into the film through the hole to the backflow away from the hole through the damper annulus.

The flow through the hole (which may also consist of a backflow through the inlet hole, especially when the lubricant pressure attains high values in proximity of the hole) depends on its hydrodynamic resistance, which is theoretically given in [52]: $\alpha_R = 128\,\mu l / \pi d^4$ (l is the orifice length).

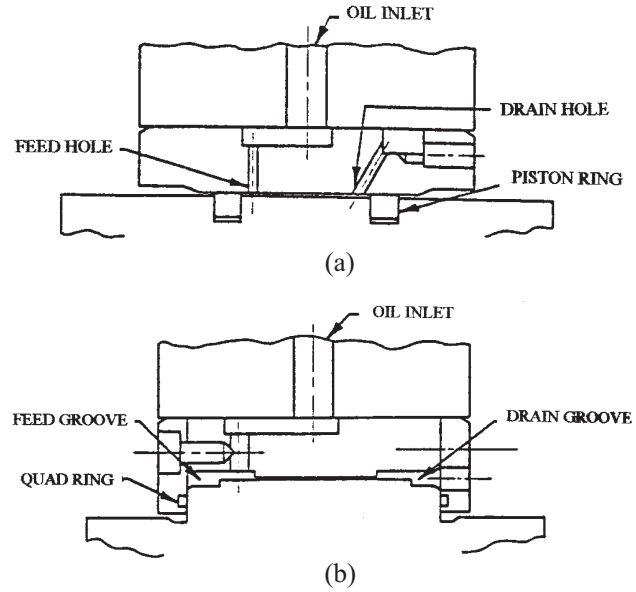

Figure 13. Examples of oil supply/outflow arrangements: (a): inlet and outlet holes with *local* seal achieved by means of *piston rings*; (b): side supply and outflow grooves with *global* seal achieved by *quad rings* in an axial arrangement (reproduced by permission of the ASME [52])

In [64] the pressure distribution in the presence of inlet holes was obtained with recourse to trigonometric series.

The lubricant outflow from the damper can be regulated by adopting an arrangement with *drain-grooves* and/or *drain-holes*, with incidental use of flow regulators (*restrictor tubes*): thus an adequate circulation of lubricant can be assured together with the assigned levels of pressure that have to be maintained in the film. The arrangement of the inlet and outlet holes can notably affect lubricant flow and the incidental presence of rupture zones [62]. The addition of grooves can sometimes avoid the undesired effects that arise when the circulation is achieved by means of holes alone [54]. Similar results can be achieved by adopting for the lubricant outflow (and sometimes also for the inlet) a seal that is suitably equipped with a series of small holes (*serrated piston ring*) [65–67]. Figure 13 illustrates two arrangements [52] where the oil supply and outflow was established both through holes and grooves, arranged laterally, for different types of seals.

4.5. The Resultant Pressure Force and the Force Coefficients

When the orbits covered by the journal within the damper bearing are exactly or nearly circular and centered and $\varepsilon' << \varepsilon\vartheta'$, the limits ϕ_1 and ϕ_2 can be assumed to depend only on the mean value of the orbit radius. Thus, under the hypothesis that the area of the cavitated zone of the film rotates with the pressure distribution, the coefficients $\overline{C}_{ij}$ can be assumed to be constant during the precession motion of the journal. The above hypothesis was confirmed by experimental tests (for instance [68]) showing the rotation of the cavitated zone with the pressure wave, even though some investigators [34, 66] noticed the persistence of gas cavities during the high-pressure portion of the cycle.

Furthermore, ϕ_1 and ϕ_2 obviously depend on the pressure values p_1 and p_2 at the film edges and the cavitation pressure p_c. An expression that can be adopted in order to determine the cavitated zone was given by Simandiri and Hahn [69]. Assuming [34] null value for the relative pressures, i.e. $p_1 = p_2 = p_c = p_a = 0$ (the subscripts indicating relative pressures were omitted), $\varepsilon' \approx 0$, and a π-film, ϕ_1 and ϕ_2 turn out to be π and 2π, respectively, once the origin of the ϕ coordinate has been fixed in the section corresponding to the maximum thickness of the film.

The determination of F_r and F_s, or C_{ij} factors, must generally be carried out through numerical procedures. Analytical expressions can be given once the SBA or LBA have been assumed for the damper. Under these hypotheses, the $\overline{C}_{ij}$ factors in equation (4) can be expressed as a function of the following type of integrals [35, 44, 70]:

$$I_n^{lm} = \int_{\phi_1}^{\phi_2} \frac{\sin^l \phi \cos^m \phi}{(1-\varepsilon \cos\phi)^n} d\phi \,. \tag{15}$$

For example, the dimensionless damping coefficients, determined for π-film [34, 35, 39] are show in Table 1.

If the film is *uncavitated*, the cross coefficients are null and the values of the direct coefficients are twice the corresponding ones relating to π-film.

If the orbit of the journal center is perfectly circular ($\varepsilon' = 0$), the components of the fluid film force can be expressed as

$$F_r = -\overline{C}_{rs}\varepsilon\vartheta' \quad F_s = -\overline{C}_{ss}\varepsilon\vartheta'. \tag{16}$$

From the first expression of (16) it can be inferred that, in the absence of cavitation, since $\overline{C}_{rs} = 0$ (whatever the L/D ratio) the SF cannot react to radial action (it is worth noting the hypothesis of absence of inertia effects). In this case, the film damper can be adopted only in the presence of elastic elements arranged in parallel with the film (Figure 6(a),(d)).

In order to give dimensional expressions to the damping factor of Table 1, the following relationships have to be taken for the SBA and LBA, respectively:

$$C_{ij} = (\mu R L^3 / C^3)\overline{C}_{ij}, \quad C_{ij} = (\mu R^3 L / C^3)\overline{C}_{ij}.$$

An example of the force coefficients relative to the *finite length* SFDs, expressed through analytical approximation (*WA*), for CCOs of the journal center, was reported in [39].

The force coefficients obtained for approximately CCOs of the journal (with respect to the bearing) can be directly adopted for rotordynamic analyses when such motion is assumed at the SFD support station. However, as was stated above, when more general conditions are to be assumed for the motion, the coefficients $\overline{C}_{ij}$ vary along the orbit, depending on both ε and ε', and numerical (time consuming) integration methods are required. Instances of the use of the coefficients given in Table 1 are given in Part II (see for example references [16, 36, 38] reported therein).

In [44] coefficients valid for synchronous centered elliptic orbits were proposed under the assumption that trajectories with this shape can sometimes approximate more closely to actual operating conditions. The coefficients were obtained with a least square method from the actual force through to a complete orbit, and were time independent.

Table 1. Dimensionless damping coefficients (π-film)

	SBA	LBA
$\overline{C}_{rr}$	$\dfrac{\pi(1+2\varepsilon^2)}{2(1-\varepsilon^2)^{5/2}}$	$\dfrac{6\pi}{(1-\varepsilon^2)^{3/2}}$
$\overline{C}_{rs}$	$\dfrac{2\varepsilon}{(1-\varepsilon^2)^2}$	$\dfrac{24\varepsilon}{(2+\varepsilon^2)(1-\varepsilon^2)}$
$\overline{C}_{sr}$	$\dfrac{2\varepsilon}{(1-\varepsilon^2)^2}$	$\dfrac{24}{(1+\varepsilon^2)(1-\varepsilon^2)}$
$\overline{C}_{ss}$	$\dfrac{\pi}{2(1-\varepsilon^2)^{3/2}}$	$\dfrac{12\pi}{(2+\varepsilon^2)(1-\varepsilon^2)^{1/2}}$

The *linearized stiffness and damping coefficients* (hints in Section 3) obtained through perturbation of the steady-state condition of the journal center (small orbits about a static position or perturbation of steady state trajectories like CCOs) satisfy the following expression, written in the absence of effects of fluid inertia:

$$\delta F_r = -a_{rr} r - a_{rs} s - b_{rr} r' - b_{rs} s'$$

$$\delta F_s = -a_{sr} r - a_{ss} s - b_{sr} r' - b_{ss} s'.$$

The perturbation of the steady-state condition is represented by the radial and tangential displacements r and s with their time derivatives. The stiffness and damping coefficients, are represented by the terms a_{ij} and b_{ij}, respectively, and examples of their expressions and use were given in [34, 39, 40, 71] and in references [13, 21, 57] of Part II [4].

5. Hydrodynamic Forces in the Presence of Fluid Inertia Effects

Unlike with journal bearings, fluid film inertia can considerably affect the pressure distribution in the lubricated clearance of an SFD and, consequently, its dynamic characteristics. The higher the value of Re*, the more pressure distributions differ from the anti-symmetrical distribution corresponding to Re* = 0, with a consequent influence on the F_r and F_s components (see, for instance, Figure 4 in [61]). A qualitative explanation *in a physical sense* was given by Tichy [38]. The main effect resulting from lubricant inertia is represented by a radial outward force, which is comparable to the effect of a *virtual mass added to the journal* and is more marked when the journal covers small amplitude orbits and the SFDs is *long* (i.e. it can be modelled with the LBA [35]). The consequent attenuation of the SFD's radial force component that is due to the presence of cavitation, gives rise to better operating conditions, with the restriction or disappearance of the operating ranges with *bistable conditions*, and a reduction in *transmissibility* (see [17, 72] and Part II). As far as the resonance curves are concerned, the beneficial effect of the fluid inertia is seen in an attenuation of the amplitude of the orbits by making the values of the critical speeds vary, particularly at the main critical speed. Furthermore, it must be pointed out that the damping coefficients also prove to be influenced by lubricant inertia: the higher Re* is, the greater is the effect. The inertia effects were considered in a number of theoretical [36–38, 41, 45, 49, 51, 57, 58, 61, 63, 72–82] and experimental investigations [13, 52, 59, 61, 65, 83–89].

The fluid motion is represented by means of the *Navier–Stokes* (*N–S*) *equations* (under the usual hypotheses for lubrication theory) with the inertia terms, and the *continuity equation*. Under the assumption of a Cartesian reference frame placed in the clearance (the curvature of which is neglected since $C << R$), the equations can be written [82]:

$$\rho\left(\frac{u}{t}+u\frac{u}{x}+v\frac{u}{y}+w\frac{u}{z}\right)=-\frac{p}{x}+\frac{\tau_{xy}}{y}$$

$$\rho\left(\frac{w}{t}+u\frac{w}{x}+v\frac{w}{y}+w\frac{w}{z}\right)=-\frac{p}{z}+\frac{\tau_{zy}}{y}$$

$$0=-\frac{p}{y}$$

$$\frac{u}{x}+\frac{v}{y}+\frac{w}{z}=0. \qquad (17)$$

By putting the terms of (17) in a suitable dimensionless form, the dependence of the inertia terms on the Re* number in particular can be clearly seen; a comparison between the respective magnitudes shows that the inertia terms can be neglected when Re* < 1 [37, 38]. With reference to F_r and F_s forces given in (2), the inertia terms can be expressed by means of the factors M_{ik} which, as they depend on Re*, are in agreement with (3).

Equations (17) represent a system of nonlinear equations that can generally be solved by means of approximated methods. "*Exact*" solutions of (17) can be obtained when the orbits of the journal center *are small with respect to the radial clearance* (see [60], p. 31). *In this case*, *the convective inertia terms* ($u\cdot\ u/\ x,\ldots$) *can be neglected* [74, 79–81] so as to make the simplified equations linear. San Andrés [60] and San Andrés and Vance [41] highlight the limits under which the above approximation can be held, showing, in particular, that the added mass effect decreases as the orbit radius increases when the full inertial terms are retained, for large amplitude orbits. A more accurate analysis [76], that treats the nonlinearity that is due to the convective unsteadiness by means of suitable linearization [90], further underlines the dependence of the damping coefficients on Re*. This characteristic is unpredicted when the convective terms are disregarded or included in the analysis with a poor approximation.

In the consulted literature, two approximate approaches were adopted in order to tackle the solution of system (17) and are known as the *momentum approximation* [35, 91] (aka *method of averaged inertia* [37, 82, 92, 93], *Von Karman integral-type analysis* or *boundary layer integral method* [51, 57]) and the *energy approximation* [35, 36, 91].

According to the first approach, the continuity and the N-S equations (17) are first integrated along the film thickness, so as to obtain the following equations [82]:

$$\rho\left\{\frac{q_x}{t}+\frac{I_{xx}}{x}+\frac{I_{xz}}{z}\right\}=-h\frac{p}{x}+\Delta\tau_{xy}$$

$$\rho\left\{\frac{q_z}{t}+\frac{I_{xz}}{x}+\frac{I_{zz}}{z}\right\}=-\left(\frac{R}{L}\right)^2 h\frac{p}{z}+\Delta\tau_{zy} \qquad (18)$$

$$\frac{q_x}{x}+\frac{q_z}{z}=-\frac{h}{t}$$

with:

$$I_{xx}=\int_0^h u^2\,dy;\ \ I_{xz}=\int_0^h uw\,dy;\ I_{zz}=\int_0^h w^2\,dy;$$

$$q_x=\int_0^h u\,dy;\ q_z=\int_0^h w\,dy;\ \tau_{xy}=\frac{u}{y};\ \tau_{zy}=\frac{w}{y}; \qquad (19)$$

$$\Delta\tau_{ij}=\tau_{ij}(y=h)-\tau_{ij}(y=0).$$

Recourse to this approximation is acceptable when the regions of the film affected by inversion of the fluid flow along the film thickness are limited [57]. In the case of CCOs, expressions similar to (19) are obtained by adopting a reference frame that rotates according to the precession of the journal in place of the fixed axes. Within this frame of reference, the lubricant flow is stationary with respect to the reference itself and the terms of (18) with derivatives $/\ t$ being null [41, 51, 73]. Neglecting the convective terms [60 (p. 46), 78] corresponds to nullifying the integrals I_{ij} in equations (18).

The solution of system (18), or the analogous one, can generally be sought by expressing the integral terms and $\Delta\tau$ the terms in the equations, after assuming that the velocity profiles in (19) are obtained in the absence of inertia [82]. San Andrés and Vance [78] pointed out that the wall shear stresses in (18) are highly dependent on the Re* number, even if the mean velocity remains constant. Thus the practice of making the wall shear stress difference dependent on the mean velocity leads to incorrect predictions being made for high values of Re*. Expressions of the integral and $\Delta\tau$ terms written with a better approximation and as a function of Re* were adopted in [41, 60]. According to the methodology illustrated therein, the pressure distribution also includes a term that explicitly depends on Re*, according to a linear relationship whose validity is restricted, strictly speaking, to the range Re* << 1. This approach can be justified by taking into account the methods for seeking approximated solutions, usually known as *perturbation methods*: assuming Re* as a parameter, equations (18) are given a small perturbation by means of expressions for the pressure distribution and the components of fluid velocities that are expanded in power series of Re* [94]. With first-order expressions the approximated solution can be assumed to be *exact* only for Re* << 1. San Andrés and Vance [41, 57] and Tichy [51] showed that the solutions obtained with small values of Re* can be held even for higher values (Re* < 25).

According to the second methodology (*energy approximation*, [35, 91]), after expressing the kinetic energy of the fluid, the inertia forces can be obtained by means of the *Lagrange equations*, in addition to the *Reynolds transport theorem*. Alternatively [36, 91], the N–S equations can be multiplied for the axial and circumferential velocities, before integrating along the film thickness. In both these two approaches, the velocity profiles along the film thickness are assumed to be those that can be taken in the absence of inertia effects.

Some results from the theoretical studies cited above are reported below and refer to the main typical conditions of

motions adopted for rotordynamic investigations, represented by orbits of the journal that are small or circular and centered.

5.1. Orbits with Small Amplitude

Different theoretical approaches, that were in accordance with the remarks made in the previous section, were adopted in order to characterize the linearized force coefficients corresponding to small motions of the journal center about an eccentric equilibrium position.

The work of Smith [95] provides an early example of insight into the theoretical problem relative to the determination of dynamic characteristics for journal bearings in the presence of inertia effects within the fluid film. The analysis resorted to a sort of two-dimensional Reynolds equation with terms explicitly depending on the components of the journal acceleration. The general *linearized* expression of the film force was given according to the *stiffness, damping and inertia coefficients* (it was noticed, in particular, that the stiffness terms are negligible).

Reinhardt and Lund [94] reported an example of design determination of the dynamic coefficients, as an applicative illustration of a theoretical analysis where the coefficients were obtained within a first-order perturbation solution in Re* (as in [79]). In particular, the inertia coefficients were numerically computed varying the static eccentricity for different *L*/*D* ratios.

Szeri et al. [37] adopted the method of the averaged inertia for moderate values of Re* (assuming wall shear stress differences obtained in the absence of inertia) under the SBA. Damping and inertia coefficients were numerically obtained for cavitated and uncavitated conditions. A comparison was drawn with the data from [94].

The theoretical approach given in [95] was resumed by Ramli et al. [75] who numerically evaluated the inertia coefficients for the *finite length* model with complete oil film. The results were compared with the approximate coefficients from [95] and the coefficients from [37, 94].

For eccentric small *circular* orbits, Tichy [80] reported *exact*, quite involved expressions of the pressure distribution, fluid film force and damping coefficients, valid under the SBA and taking into account the *visco-elasticity* of the lubricant. A basis for the theoretical development was represented by a number of previous studies about the squeeze film in oscillating surfaces or bearings [74, 96–98]. In the analysis, the convective inertia terms were neglected and a stream function was adopted for expressing the velocity components. The four total coefficients obtained included inertia effects and were plotted against mean eccentricity, for full-film conditions and different sets of Re* and De (De is the dimensionless *Deborah* number for characterizing the visco-elastic behavior), through numerical integration.

San Andrés [60] and San Andrés and Vance [78], for the *finite length* SFD, solved mean flow equations similar to equations (18), neglecting the *convective* terms, with a procedure that provided results accurate for Reynolds number up to values of 25. The wall shear stresses were written with terms containing Re* and a function of the velocity fields that could be given simple, approximated expressions only for the LBA and SBA. After assuming a linear dependence of the pressure from Re*, the obtained set of partial differential equations was numerically integrated and *exact* dynamic coefficients were obtained.

Table 2. Dimensionless damping and inertia coefficients (2π-film, small orbits with mean eccentricity ε)

	SBA	LBA
$\bar{C}_{rr}$	$\dfrac{\pi(1+2\varepsilon^2)}{(1-\varepsilon^2)^{5/2}}$	$\dfrac{12\pi}{(1-\varepsilon^2)^{3/2}}$
$\bar{C}_{ss}$	$\dfrac{\pi}{(1-\varepsilon^2)^{3/2}}$	$\dfrac{24\pi}{(2+\varepsilon^2)(1-\varepsilon^2)^{1/2}}$
$\bar{D}_{rr}$/Re*	$\dfrac{\pi}{5}\dfrac{1-(1-\varepsilon^2)^{1/2}}{\varepsilon^2(1-\varepsilon^2)^{1/2}}$	$2.4\pi\dfrac{1-(1-\varepsilon^2)^{1/2}}{\varepsilon^2}$
$\bar{D}_{ss}$/Re*	$\dfrac{\pi}{5}\dfrac{1-(1-\varepsilon^2)^{1/2}}{\varepsilon^2}$	$2.4\pi\dfrac{1-(1-\varepsilon^2)^{1/2}}{\varepsilon^2}$

In the above investigations, approximate, closed-form expressions were further suggested for the coefficients. These approximate expressions were strictly valid for low values of Re* but proved to be surprisingly accurate for Re* up to 25. Since Re* < 10 in most practical applications, the approximate coefficients are very useful. Tichy [80] reported four approximate analytical total linearized coefficients, corresponding to the *exact* ones (see above), valid for SBA and 2π-film, and found them to be accurate in the range Re* < 20, De < 1.5. A broad set of approximate linearized coefficients, valid for SBA and LBA, and π and 2π film, was given by San Andrés and Vance [78]. The inertia coefficients were derived from [74, 80, 81, 94], while the damping coefficients, distinct from those of inertia, coincided with the classic ones determined from the Reynolds equation in the absence of inertia effects. As an example, the coefficients valid for 2π-film conditions are shown in Table 2. Approximate expressions for the *finite length* SFD, in a *WA* form, were also given in [78].

The case with small circular centered orbits (CCOs) can be assumed as a particularization of the previous case. Tichy [81] studied this condition for the LBA and 2π-film, in line with the analysis carried out for small off-center orbits. The amplitude F of the whole squeeze film force and its angle of application ψ (Figure 14) were given the following approximated expressions:

$$F \cong F_1\left[1+(\mathrm{Re}^*/10)^2\right]^{1/2};$$

$$\psi = \pi/2+\tan^{-1}(\mathrm{Re}^*/10). \tag{20}$$

The *correction* terms depending on Re* in relationships (20) represent the effect of fluid inertia that *changes the amplitude* F_1 of the pure viscous force, corresponding to the inertialess conditions, and its *original tangential direction*. Comparison with more accurate data from an *exact* theoretical analysis showed that relationships (20) turned out to be accurate for Re* up to 25.

In [77] the *exact* theory for the *finite length* damper and small off-center orbits was recast for centered motion by means of analytical approximations that avoided recourse to the mean flow equations. The tangential and radial force components showed their dependence on the only direct

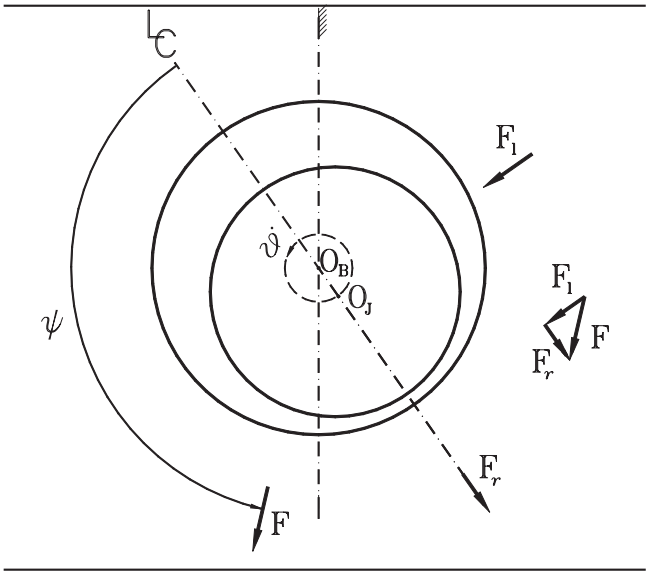

Figure 14. Total fluid film force with small centered orbits and uncavitated film, in the presence of inertia effects in the lubricant

Table 3. Expressions of the fluid film action (2π-film, CCOs, orbit radius $e << c$) [35]

	SBA	LBA
F_s	$-\pi\mu e\omega \frac{RL^3}{C^3}\left(1+\frac{\mathrm{Re}^{*2}}{8400}+...\right)$	$-12\pi\mu e\omega \frac{R^3L}{C^3}\left(1+\frac{\mathrm{Re}^{*2}}{8400}+...\right)$
F_r	$\pi\mu e\omega \frac{RL^3}{C^3}\frac{\mathrm{Re}^*}{10} \times\left(1-\frac{11}{907200}\mathrm{Re}^{*2}+...\right)$	$12\pi\mu e\omega \frac{R^3L}{C^3}\frac{\mathrm{Re}^*}{10} \times\left(1-\frac{11}{907200}\mathrm{Re}^{*2}+...\right)$

Table 4. Dimensionless inertia coefficients (CCOs, 2π-film, small Re* << 1) [1]

	SBA	LBA
$\bar{D}_{rr}$ / Re*	$-\frac{1}{6}\pi\frac{[\sqrt{1-\varepsilon^2}-1]}{\varepsilon^2\sqrt{1-\varepsilon^2}} \times\left[-\frac{12}{7}+\frac{102}{35}\sqrt{1-\varepsilon^2}\right]$	$\frac{12}{35}\pi \times\frac{\sqrt{1-\varepsilon^2}(20+\varepsilon^2)-3\varepsilon^2-6}{(2+\varepsilon^2)^2}$

tangential damping coefficient and direct radial inertia coefficient, respectively. The approximate expressions of these coefficients, obtained for Re* → 0 and valid in the extended range 0 < Re* < 25, showed that the result expressed by (20) could be extended to the more general case of the *finite length* damper. As a matter of fact, the tangential force of the oil-film turned out to be practically independent from inertia effects for Re* approximately less than 20, while the radial force was appreciably dependent on fluid inertia and turned out to be predominant for Re* > 10. It is worth noting that the approximate relationships are coinciding with those obtained for off-center motions when the small orbits approach the centered position. Further, in these circumstances, the analytical relationships for the SBA and LBA indicate that the cross-coupling coefficients approach zero.

El-Shafei and Crandall [35] showed that relationships (20) represented the first terms of a general linearized solution, obtained from linearized N–S equations and valid under the assumptions of orbit radius $\varepsilon << 1$ and $C/R << 1$. The corresponding radial and tangential forces, for the SBA and LBA, are shown in Table 3. These approximate relationships were compared with the exact ones obtained through the energy approximation and proved to be accurate in the range 0 < Re* < 16. However, the expressions of F_r in Table 3 suggest that the inertia effect was greater in the *long* model than in the *short* one. The *added mass* due to the effect of fluid inertia was in fact about R/C times and $(R/C)[L^2/(12R^2)]$ times the mass of the fluid film in the LBA and SBA cases, respectively.

5.2. Exact or Approximately Circular Centered Orbits

When the hypothesis about the smallness of the motion amplitude is removed, the convective terms in the N–S equations cannot be disregarded. In [78] it was remarked that the linearized inertia coefficients (as obtained for small amplitude orbits) are not to be used for circular centered motions of large amplitude in order to correctly predict the reduction in the added mass effect with the increase in the orbit radius, as a result of the effect of the convective fluid inertia.

Characterization of the SFD behavior in the presence of journal CCOs and fluid inertia effects has been carried out in [41, 51, 57, 60, 73, 76]. Under the hypothesis of CCOs, most analyses adopted a reference frame (r, s) rotating with the (constant) angular speed corresponding to the precession motion of the journal center. With respect to this reference the flow is stationary and no time derivatives appear in the equations of motion.

In [41] the N–S and continuity equations were integrated along the film thickness, and the field of velocity and the pressure distribution were solved by means of a perturbation technique, expanding the solution in powers of Re*. The velocity momentum integrals (see (19)) were written under the assumption that the shape of the velocity field was not greatly affected by inertia (from small to moderate values of Re*) and the wall shear stresses were expressed as a function of the mean flow rates, with a further explicit contribution of inertia that was suitably evaluated from case to case. Expressions of the direct damping coefficient C_{ss} and the direct radial coefficient D_{rr} were obtained for the SBA and LBA, under full-film conditions (the cross-coupled coefficients were null), for both laminar and *turbulent* regimes. The damping coefficient was the same as that in the inertialess solution, while the inertia coefficient was given different analytical approximated expressions depending on Re* (Re* << 1, Re* → ∞, moderate Re*). As an example, the inertia coefficient valid for small values of Re* (Re* < 1) and laminar conditions is shown in Table 4.

A similar approach was carried out in [57] for *finite length* SFDs. On the one hand, the mean flow equations were numerically solved with a *finite element method* (*FEM*) based procedure that led to *exact* coefficients valid for Re* up to about 10 (the hypothesis that the shape of the velocity profiles was not greatly affected by inertia was assumed). However, approximate analytical results were obtained with a treatment that exhibited some analogies with the approach

Table 5. Inertia coefficients for approximately circular orbits (π-film) [35]

	SBA	LBA
$M_{r\,\mathrm{rad}}$	$\frac{\pi}{10\varepsilon^2}[(1-\varepsilon^2)^{-1/2}-1]$	$\frac{12\pi}{10\varepsilon^2}[1-(1-\varepsilon^2)^{1/2}]$
$M_{r\,\mathrm{non}}$	$\frac{17\pi}{70\varepsilon^2}\left[2-\frac{2-3\varepsilon^2}{(1-\varepsilon^2)^{3/2}}\right]$	$-\frac{12\pi}{70\varepsilon^2}\left[1-\frac{2-\varepsilon^2}{2(1-\varepsilon^2)^{1/2}}\right]$
$M_{r\,\mathrm{tan}}$	$-\frac{1}{10\varepsilon}\left[2+\frac{1}{\varepsilon}\log\left\lvert\frac{1-\varepsilon}{1+\varepsilon}\right\rvert\right]$	$\frac{12}{10\varepsilon}\left[2+\frac{2(1-\varepsilon^2)}{\varepsilon(2+\varepsilon^2)}\log\left\lvert\frac{1-\varepsilon}{1+\varepsilon}\right\rvert\right]$
$M_{r\,\mathrm{cor}}$	$\frac{1}{70\varepsilon}\left[20+\frac{27}{\varepsilon}\log\left\lvert\frac{1-\varepsilon}{1+\varepsilon}\right\rvert+\frac{31}{1-\varepsilon^2}\right]$	0
$M_{r\,\mathrm{cen}}$	$\frac{\pi}{70\varepsilon^2}\left[27-\frac{27-17\varepsilon^2}{(1-\varepsilon^2)^{1/2}}\right]$	$\frac{1.2\pi}{(2+\varepsilon^2)^2}\left[12-\frac{2(10-\varepsilon^2)(1-\varepsilon^2)^{1/2}}{2+\varepsilon^2}\right]$
$M_{s\,\mathrm{rad}}$	$-\frac{1}{10\varepsilon}\left[2+\frac{1}{\varepsilon}\log\left\lvert\frac{1-\varepsilon}{1+\varepsilon}\right\rvert\right]$	$\frac{12}{10\varepsilon}\left[2+\frac{2(1-\varepsilon^2)}{\varepsilon(2+\varepsilon^2)}\log\left\lvert\frac{1-\varepsilon}{1+\varepsilon}\right\rvert\right]$
$M_{s\,\mathrm{non}}$	$\frac{17}{70\varepsilon}\left[2+\frac{2}{\varepsilon}\log\left\lvert\frac{1-\varepsilon}{1+\varepsilon}\right\rvert+\frac{2}{1-\varepsilon^2}\right]$	$\frac{12}{10\varepsilon}\left[\frac{(2\varepsilon^4-10\varepsilon^2-4)}{\varepsilon(2+\varepsilon^2)^2}\log\left\lvert\frac{1-\varepsilon}{1+\varepsilon}\right\rvert-\frac{4}{2+\varepsilon^2}\right]$
$M_{s\,\mathrm{tan}}$	$\frac{\pi}{10\varepsilon^2}\left[1-(1-\varepsilon^2)^{1/2}\right]$	$\frac{1.2\pi}{\varepsilon^2(2+\varepsilon^2)}\left[\frac{4(1-\varepsilon^2)^{3/2}}{2+\varepsilon^2}+5\varepsilon^2-2\right]$
$M_{s\,\mathrm{cor}}$	$\frac{\pi}{10\varepsilon^2}\left[-\frac{27}{7}-(1-\varepsilon^2)^{1/2}+\frac{17}{7}\frac{2-\varepsilon^2}{(1-\varepsilon^2)^{1/2}}\right]$	$\frac{1.2\pi}{(2+\varepsilon^2)^2}\left[12-\frac{2(10-\varepsilon^2)(1-\varepsilon^2)^{1/2}}{2+\varepsilon^2}\right]$
$M_{s\,\mathrm{cen}}$	$-\frac{27}{70\varepsilon}\left[2+\frac{1}{\varepsilon}\log\left\lvert\frac{1-\varepsilon}{1+\varepsilon}\right\rvert\right]$	$m_{22}^{*}-\frac{12}{10}\frac{\varepsilon(8+\varepsilon^2)}{(2+\varepsilon^2)^2}$

$$m_{22}^{*}=\frac{27}{35}\varepsilon\left[-\chi^3/\Lambda^2+\eta^3/\Sigma^2\right]+\frac{3}{5}\left[\chi^2/\Lambda-\eta^2/\Sigma\right]$$

$$\chi=\frac{3\varepsilon}{2+\varepsilon^2}-1;\quad \eta=\frac{3\varepsilon}{2+\varepsilon^2}+1;\quad \Lambda=1-\varepsilon;\quad \Sigma=1+\varepsilon$$

given in [78], where the pressure was expressed as the sum of a zeroth order, purely viscous flow solution plus a first order, inertial pressure field depending on Re*. The analytical approach made it possible to take into account the finite length of the damper (different *L/D* ratios were assumed) plus the possible presence of locally end-sealed conditions. The direct and cross-coupling coefficients C_{ss}, C_{rs}, D_{rr} and D_{rs} were presented for π-film conditions and different *L/D* ratios.

The above theoretical schemes assumed tangential damping forces constant with Re*. The theoretical analysis of Tichy and Bourgin [101] and the experimental one of San Andrés [102] showed that the dependence of the damping forces on fluid inertia, for large orbit radii, was not null. In this respect, San Andrés [76] presented a numerical procedure (finite difference method) through which the convective terms were expressed with a second order approximation [90]. For the case in question (LBA with full-film conditions) the tangential force depended merely on the damping action, but the C_{ss} coefficient was different with respect to the pure viscous case and showed values that increased with Re*: when Re* = 50 the increases compared to the viscous solution were 20% for $\varepsilon = 0.75$ and 23% for $\varepsilon = 0.01$.

In the case of approximately CCOs of the journal center, El-Shafei and Crandall [35] obtained ten inertia coefficients M_{ij} (according to relationships (3)) valid for Re* in a range consistent with the ordinary SFD applications. Their expressions, particularized for SBA or LBA, and π-film conditions, are shown in Table 5 (for uncavitated conditions, the coefficients $M_{r\mathrm{rad}}$, $M_{r\mathrm{non}}$, $M_{r\mathrm{cen}}$, $M_{t\mathrm{tan}}$, $M_{t\mathrm{cor}}$ are twice the respective ones in Table 5, while the others are null. In the case of cavitated film El-Shafei and Crandall stressed though the need to determine the effective size of the cavitated zone of the film since it is influenced by the lubricant inertia as well as other factors).

These coefficients were obtained through the *energy approximation* that took into account the kinetic coenergy of the fluid. The Lagrange equation and the Reynolds transport theorem allowed the expression of two terms, respectively, that constituted each force component (in this scheme, the velocity profiles were assumed the same as those for the inertialess case). It was shown that a difference of about 20% resulted when comparing the coefficients obtained by the *energy* and *momentum approximations* (the latter method was adopted in [91]). The results corresponding to the limit case of small CCOs, namely the linearized coefficients (see the previous section), agreed with the theoretical data from other investigations.

Zhang et al. [36] compared different approximated methods (particular attention was given to the *momentum* and the *energy approximations*) and pointed out that the inertia coefficients can share the same formal expressions from method to method, the only differences being the numerical values of two constants that depend on the averaging methods used in each procedure. Focusing on the SBA case with uncavitated film, they underline the temporal and convective contributions to the inertia coefficients. In particular, the importance of the convective terms at higher orbit radii was suitably noted.

Instances of the use of the inertia coefficients are given in rotordynamic investigations referred to in Part II (see for example references [50–53, 64] reported therein).

6. Experimental Investigations

In order to experimentally estimate the hydrodynamic action in the damper and the related dynamic coefficients, both free [59, 71, 86, 87] and, to a greater extent, forced relative motions were imposed to the journal-bearing pair of the SFD.

It is worth noting that this standpoint, in line with the theoretical investigation illustrated in the previous sections, differs from the point of view that characterizes the analyses referred to in Part II [4], where the relative motion of the journal-bearing pair of the SFD was an output of the system (i.e. a rigid or flexible rotor with assigned imbalance to be examined).

In particular, the constrained motion assumed in [84] was translatory, while orbital motions were imposed by means of the eccentric drive of the journal itself [13, 46–48, 52, 58, 61, 65, 67, 88, 103–106] or excitation along two perpendicular directions [34, 107]. Off-centered orbits were dealt with in [46–48, 85, 108]. It is worth noting that, in the case of an eccentric drive, the effective radius of the orbits of the journal center must be checked because its actual values could be considerably influenced by the operating parameters (speed and viscosity; see [13, 52]).

In most cases, the experimental pressure distributions represented the basis for calculating the fluid film force. Many authors reported the measured radial and tangential components [13, 46–48, 58, 60, 65, 73, 88, 103] or the correspondent dynamic coefficients [60, 61, 67, 104, 105] as they were obtained from numerical integration of the pressure data. Sometimes a direct measure of the forces was carried out with piezoelectric force gauges or strain gauges. In these cases the sensors could either detect the reaction of the film corresponding to the imposed motion [52, 106] or measure the force directly applied to the mobile member (journal or bearing) of the SFD, by means of hydraulic [34, 54] or electromagnetic [107] shakers.

In particular, with regard to the experimental coefficients for the film force, besides the damping coefficients, inertia coefficients were evaluated in [52, 60, 61, 67, 84, 85, 104, 105, 107] and stiffness coefficients in [84, 85, 107]. A comparison between two methods for the evaluation of the dynamic coefficients was shown in [83]. In [85] a method of parametric identification was adopted in order to determine the complete set of twelve linear hydrodynamic coefficients for the SFD.

A circumferential groove arranged laterally with respect to the film for the supply of lubricant was adopted in [46, 47, 58, 67, 103, 108]. The groove was centrally placed (in the middle plane of the SF) in [54, 59–61, 71, 84–87, 107]. A centrally arranged hole for the inlet flow was adopted in [48, 106] while lateral feed holes provided the arrangements in [13, 65, 67, 88, 104, 105]. In [52] the film was fed in two different ways by adopting end inlet holes or an end groove, respectively (Figure 13). The outlet of the lubricant was realized by means of a lateral circumferential drain groove in [13, 58, 65, 88, 103, 108] or calibrated lateral holes in [46, 47, 104, 105]. In [73, 106] the SFD was submerged. Conditions with flooded damper were also examined in [34].

As far as the lack or presence of seals was concerned, open end conditions were realized in [13, 58, 59, 67, 84–86, 88, 104, 107, 108]. Experimental tests with partially sealed SF were carried out in [13, 65, 67, 103, 105]. Totally (or globally) sealed conditions characterized the arrangements adopted in [34, 46–48, 52, 54, 61, 106].

With regard to the geometry of the bearing, experimental L/D ratios in the range $0.15 \div 0.25$ were generally adopted. Higher ratios characterized the dampers in [34] (0.5, 0.75), in [48] (0.96) and [61] (0.94). In most part of the analyses, the C/R ratio was assigned in the interval $0.001 \div 0.01$, while a C/R ratio of about 0.025 was realized in [48, 61, 65, 88, 104–106] (the resulting values of C were consistent with the presence of inertia effects).

By and large, from a qualitative point of view the results of the referred experimental investigations confirm the theoretical predictions summarized in the previous sections. An overview of the experimental work is presented below, with particular reference to the observation of the *pressure distributions*, with the possible presence of cavitating conditions, and the measurement of the *film forces* and the related dynamic coefficients.

6.1. Pressure Distribution and Cavitating Conditions

A good deal of experimental work has been devoted to evaluating the pressure distribution within the film. Different types of film behavior were recognized with reference to the capability of sustaining the pressure distributions connected to the journal motion, depending on the arrangements adopted for the oil supply and drain, the level of the inlet pressure, the possible presence of seals, etc.

Piezoelectric type pressure transducers have frequently been adopted [13, 34, 58, 65–67, 88, 104, 105]. The pressure distributions were obtained as *dynamic* pressure or *pressure waves* detected by one or more pressure probes located at specific circumferential and axial positions. In many cases, a correct indication of the *absolute* pressure, especially in order to establish the actual value of the pressure in the region of cavitation, was possible thanks to specific probes of the *absolute* type, generally represented by *strain-gauge* sensors [103–105]. In some investigations the absolute pressure transducer was capable of both *static* and *dynamic* pressure measurements (for instance, in [68] the investigators used a miniature *diaphragm* sensor with strain gauge conditioner; see also [48, 109]). In [34, 54, 62, 66] direct *flow visualization* was carried out. Except for the tests in [62], the direct observation was supported by a measure of the pressure distributions. In [54] the extent of

the cavitated zone was appreciated with recourse to a *fiber optic probe*, in addition to the pressure sensor (the pressure signal proved more reliable in detecting the zone affected by cavitation).

The main results from some outstanding experimental investigations about the phenomenon of cavitation, in steadily and dynamically loaded journal bearings [110–116] (for a broader literature survey the reader is referred, as an example, to Paydas [117]), represented guidelines for understanding the behavior of cavitated SFs. The mechanisms giving rise to cavitation and the consequent possible values of cavitation pressure, their effect on the aspect and position of the cavitated zone within the film and the resulting pressure distribution and the force components of the SF, were the main aspects covered by the experimental work. One of the most remarkable conclusions of this part of the study was the recognition of the inadequacy of the harsh recurrent classification regarding *unpressurized* or π-*film* and *pressurized* or 2π-*film* conditions, in order to represent the whole possible operating conditions of a SFD.

Zeidan and Vance [118] very well summarized the possible operating conditions of a damper film, with regard to rupture. They indicated five possible different regimes, as inferred from experimental pressure waves and photographs: *Regime I: uncavitated* 2π-*film*; *Regime II: cavitation bubble following the journal; Regime III: oil-air mixture; Regime IV: vapor cavitation*; *Regime V: vapor and gaseous cavitation*. The laboratory tests were carried out with a *controlled orbit* test rig, at fixed orbit radius (dimensionless eccentricity equal to 0.45). The SFD had a lateral circumferential feed groove with four inlet holes, and serrated piston rings delimited the film on both sides. The above five regimes were detected in turn, from *I* to *V*, with increasing the speed of operation. The supply pressure was suitably adjusted with assigning 3 psig in regimes *I* and *II*, 3 and 25 psig in regime *III*, 25 and 40 psig in regimes *IV* and *V*. In each of the cases from *II* to *V*, the distortion of the pressure distribution with respect to that of the pure viscous (i.e. without effects of inertia) uncavitated film, and its effect on the resultant reaction of the film, was suitably pointed out.

Figure 15 (from [67]) compares the pressure waves relative to *vapor* or *gaseous cavitation*, obtained with operation at medium eccentricities (orbit radius equal to 0.4 – 0.5, see Figure 15(a)) and high eccentricities (orbit radius equal to 0.7 – 0.75, see Figure 15(b)). In either case, the vapor regime corresponded to higher supply pressures.

Gaseous cavitation, i.e. the presence of cavities in the rupture zone, originating from air entering the damper or by the release of air and gas dissolved within the lubricant, with pressure levels that are very close, but lower than, atmospheric pressure, corresponds to Regimes *II* and *III* referred to in [118]. Typical pressure waves (Figure 15; see also [34], p. 8/26), with respect to the pressure distribution relative to uncavitated conditions, show a characteristic extension of the low-pressure region, with consequent delay in pressure build-up, reduction in the circumferential extension of the positive pressure region and downstream shift of the positive pressure peak.

Vapor cavitation conditions, coinciding with those of Regime *IV* and, partially, of Regime *V* reported in [118], are characterized by the presence of cavities originating as boiling of the lubricant at almost zero absolute pressure.

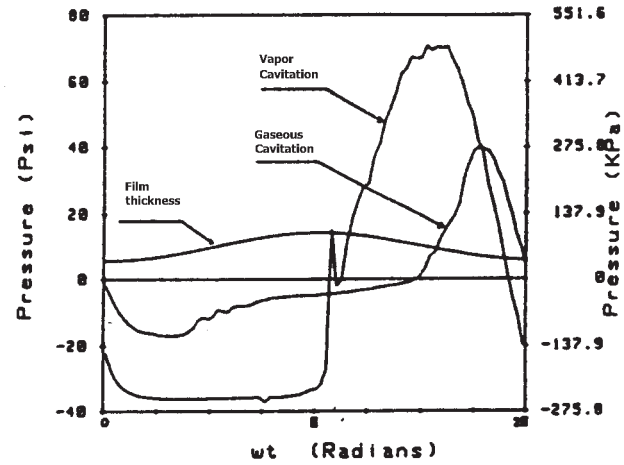

(a)

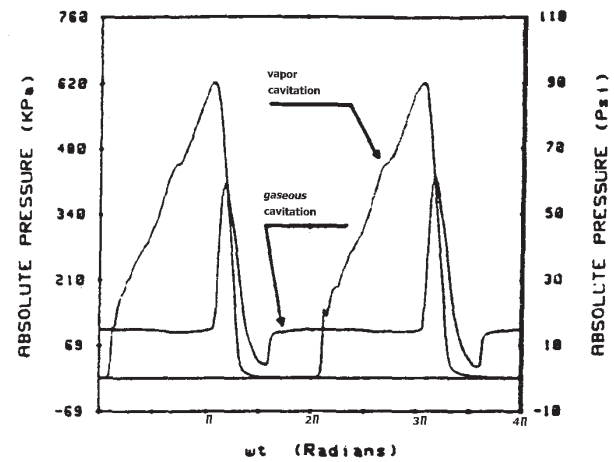

(b)

Figure 15. Comparison between pressure distributions, in the presence of vapor and gaseous cavitation. (a) Medium values for the radius of the CCOs ; (b) high values for the radius of the CCOs (reproduced by permission of the ASME [67])

The flat response in the cavitated zone (Figure 15), the subsequent quick recovery of the pressure with a steep rise – consistent with the sudden collapse of the vapor cavities that, under some conditions, is so sharp as to give rise to an overshoot – and the conservation of the positive pressure region in the convergent part of the clearance (apart from the effects of fluid inertia) are typical features of this mechanism of film rupture.

Gaseous cavitation was also observed in [34, 66, 67, 107, 119]. Air entrainment was responsible for the onset of cavitation in the laboratory tests carried out by Zhang et al. [107] for operation with journal eccentricities higher than 0.5, in the absence of end seals and moderate levels of supply pressure. White [34] described conditions with one edge of the film exposed to the atmosphere and characterized by the presence of "*entrained air of dendritic form with fingers running axially into the film*". The author sometimes observed this mechanism of cavitation in addition to circular bubbles that were persistent in the high-pressure region

(presumably as a co-existence of Regimes *II* and *III* indicated in [118]). In the presence of an end seal (and eccentricity greater than 0.4) White observed the simultaneous presence of vapor cavities and retained air bubbles (according to Regime *V*), the latter capable of surviving in the high-pressure region and the former collapsing immediately in the same region.

Vapor cavitation was detected in [46, 58, 68, 103, 104, 105]. Feder et al. [46] found cavitating pressures below the ambient pressure ($-13 \div -18$ psig), experimenting with O-ring sealed SFD and different levels of the inlet pressure. Ku and Tichy [68] measured zero absolute pressure in the cavitation region. Their attention was particularly addressed to the observation of the pressure gradient at the starting and ending boundaries of the cavitated zone, in order to evaluate the applicability of the JFO (Jacobsson–Floberg–Olsson) cavitation boundary conditions. Jung et al. [104, 105] observed vapor cavitation both for open-ended and partially sealed film conditions. In the first circumstance, the tests showed the presence of cavitation only with the highest value of the two assigned orbit radii ($\varepsilon = 0.8$) and the authors found that the more appreciable the effects of inertia, the smaller the extent of the cavitated region (the cavitation vanished when Re* was given the highest value of 22.1). For partially sealed operation the presence of cavitation was more evident, with a larger extent of the cavitated region within the pressure distributions. The rupture of the film grew with the orbit radius ($\varepsilon \approx 0.5, 0.8$) and was more persistent at increases in the Reynolds number, with respect to the case of the open-ended conditions. When comparing the cavitated regions for open-end and partially sealed conditions, Arauz and San Andrés [13] observed that the extent was larger in the first case, unlike the data from [104, 105]. This result was explained by the fact that lower supply pressures, larger orbit radius and higher oil viscosity, with respect to the case of the partially sealed SFD, characterized the operation with the open-end SFD.

Zeidan and Vance [66, 67] checked experimentally the operating conditions that led to *gaseous* or *vapor* cavitation. The latter type of cavitation could arise only for high supply pressure values and was observed with very tight seals, which is quite an unusual feature in normal engine applications. Different SFD performance was observed depending on the type of cavitation. After *gaseous* cavitation had set in, the maximum pressure at first increased with whirl velocity and then decreased with further increases in whirl speed because of the presence of a two-phase homogeneous compressible mixture of oil and air, owing to *air entrainment*. In addition, some of the air bubbles appeared to remain in the same zone of the film, regardless of the whirl motion (as observed by other investigators). Only for small velocities did the whole cavitated region rotate with the journal whirl. On the other hand, *vapor* cavities appeared only for the negative portion of the pressure wave and disappeared or collapsed at high pressures. Appearance and collapse of the vapor thus appeared to be synchronous with the rotating pressure distribution. The maximum pressure was higher than in the case of *gaseous* cavitation.

Cavitation that is due to *air entrainment* in open-end SFDs, with the rise of bubbly or foamy mixtures, has been the focus of much recent research [120–126]. Such conditions have been recognized to be quite distinct with respect to gaseous cavitation manifesting with a single large bubble of air. Yet bubbly cavitation turns out to be very frequent in practical applications. The main trouble with this cavitation mechanism is that it cannot be tackled with the common cavitation models. One reason is the fact that the oil–air mixtures can affect as dispersed bubbles, in a pervasive and complex manner (spatial and temporal fluctuations affect the bubbly zones), all the film with the inclusion of the high-pressure regions. Characterization of the presence, motion and main parameters (like viscosity) of the mixture is quite difficult. Thus an effective theoretical prediction for the degradation of damper performance due to this cavitating mechanism is somewhat problematic. The extensive investigation referred to in the cited papers entailed setting up useful theoretical models (a modified Reynolds equation for homogeneous bubbly mixture was proposed and experimentally validated. Some results are synthesized in the next section) and will probably take further work.

Full film conditions characterized by the absence of cavitation – achieved thanks to a suitable regulation of pressurization, seal effect, eccentricity of the operation (both centered or eccentric controlled orbits were studied) and frequency of the whirl – were tested in [47, 48, 61, 88]. In the last two works, these conditions allowed a better study of inertia effects (the cavitation was intentionally prevented). The occurrence of *negative absolute pressures*, with a region of the film interested by *tensile stresses*, was observed in uncavitated SF, similarly to what was reported in earlier experimental analyses regarding dynamically loaded journal bearings [114]. Such film conditions were detected in [33, 108, 127–129]. Most of these investigations regarded rotordynamic evaluation of the SFD behavior and have thus been dealt with in [4], together with other studies that also evidenced the influence of cavitating conditions onto the dynamics of SF supports–rotor systems [119, 130].

Della Pietra [108] obtained pressure distributions characterized by the presence of *tensile stresses* (up to 220 kN/m^2) for both *full* and *partially cavitated* conditions. The investigation experimentally tested an analytical expression for film pressure in the presence of moderate values of the static eccentricity of the journal. The effect of the oil feed conditions (oil pressure within the feeding groove and oil flow rate) on pressure distribution was also examined.

Walton et al. [62] observed the film rupture for a sealed SF in the presence of different supply conditions. When a feeding groove was adopted, the film rupture also affected the region with the groove. The operating speed at which cavitation arose increased with the supply pressure and decreased with journal eccentricity. When the oil supply was realized by means of inlet and outlet holes, the cavitated zone appeared to be greatly influenced by the presence of the holes and the data repeatability was not the same as when a groove was present.

The investigation of Kinsale [73] was mainly focused on inertia effects. The experimental pressure distributions showed good agreement with theoretical data obtained with numerical procedure, for orbits characterized by $\varepsilon = 0.2$, 0.4 and Re* up to 15. The study confirmed the effects of the fluid inertia about destroying the symmetry of the pressure distribution, but left aside other aspects like cavitation.

6.2. Forces and Damping Coefficients

In most cases, the experimental pressure distribution, corresponding to an assigned relative motion between the journal and the bearing of the SFD (generally CCOs), represented the basis for the determination of the fluid film force. Many authors have reported the radial and tangential components, as obtained from numerical integration of the pressure data, or the corresponding dynamic coefficients. In some analyses, the forces were directly measured with piezoelectric force gauges or strain gauges. In these cases the sensors could either detect the reaction of the film corresponding to the constrained motion [106] or measure the force directly applied to the mobile member (journal or bearing) of the SFD, by means of a hydraulic [54] or electromagnetic [107] shaker.

Early experimental analyses were often effective in showing the existence of conditions where the classic lubrication theory was satisfactory (as in [46]) or needed considerable improvements in order to give better predictions (examples can be found in [34, 48, 52]). As a result, according to theoretical investigation surveyed in the previous sections, in more recent investigations, the influence of inertia, cavitation, damper geometry and oil supply on the film forces was given specific attention.

Tichy [106] tested operating conditions characterized by values of Re* up to 13 and found a qualitative agreement between the measured forces and those obtained with theoretical models [38, 93] that took into account the inertia forces in the lubricant. The author noticed that the resulting uncertainty (± 20 percent) of the theoretical prediction was in part due to the possible effect of the seals.

San Andrés [60] noted the importance of inertia effects particularly when the geometry of the film was not oversimplified, as in a number of investigations, but characterized by the presence of discontinuities, like central and end grooves. The observation that "the dramatic effect that fluid inertia has on the interface groove-squeeze film lands, and consequently in the entire flow", was particularly related to the experimental results obtained with test-SFDs realized with central and end grooves, plus additional end journal plates, that showed radial forces (that were present as inertia effect) larger than the damping forces, for values of Re* as low as 3. These aspects made the author point out the need for improved theory, with careful treatment of the boundary conditions and a less simple expression of the wall shear stress differences. By contrast, a good correlation between experimental and predicted values of the forces was found when a more simple geometry characterized the boundary of the film.

San Andrés and Vance [61] tested an SFD provided with a central groove and side O-ring seals, operating with = 0.5 and Re* in the range 2–6. The direct damping and inertia coefficients were evaluated and the agreement with the theoretical predictions (LBA from [60] and inclusion of convective terms) turned out to be better in the case of the inertia coefficient than in the other case. The role played by the circumferential groove with regard to the influence of the inertia was pointed out, underlining the inadequacy of the assumption of constant pressure at the groove location.

San Andrés et al. [88] studied an open-ended SFD, provided with oil supply at one end, operating with uncavitated, pressurized film and $\varepsilon = 0.5$. The measured forces turned out to be underestimated by means of the adopted theory (SBA and full film conditions [41]). The radial force, in particular, was appreciably higher (with a factor approximately equal to π) than the corresponding theoretical predictions, while the tangential force showed a better agreement with the respective theoretical data, though only for low Re*. These deviations made the authors stress the need for a less simplified theory, capable of better treatment of the entrance and discharge effects with fluid inertia.

Arauz and San Andrés [13] carried out tests for open end and partially sealed conditions. CCOs with an assigned radius were adopted and the effects of varying the orbit frequency and the oil viscosity on the film force were evaluated. The experimental conditions were characterized by poor inertia effects and the measured force components were theoretically checked with the corresponding analytical expressions from the isoviscous, full film theory and the numerical data from a finite element routine [57] (in the latter better predictions were achieved). The comparison showed that the experimental tangential forces were higher than the predicted values for sealed conditions and lower than the theoretical data for open conditions. For the latter conditions, a possible cause of this discrepancy was attributed to the axial variation of oil viscosity, due to the temperature gradients. The authors observed a dependence of the tangential force on the oil viscosity that was not linear, unlike the theoretical predictions. An almost null radial force, independent of viscosity (as long as the film was uncavitated) was consistent with the theoretical expectations relative to the actual operating condition. The investigation was further effective in showing the effects of cavitation on the force components and the capability of the piston ring seal to obtain larger tangential forces with respect to the open-end configuration, while maintaining a sufficient level of oil circulation. In other tests [58] the same authors pointed out the influence of grooves. The results agreed with the theoretical predictions and showed that the order of magnitude of the dynamic pressures originating in the circumferential groove was the same as the film pressures in the damper land. Consequently, the tangential force in the groove considerably increased the damping action. Furthermore, the high values of Re* in the groove made the contribution to the radial force comparable with the action that was merely due to the film damper, whose Re* number was close to one (C and C/R were the same as in [13]). The authors inferred that the presence of the groove was responsible for a sort of inertia effect on damper performance. This investigation, carried out for open-end conditions, was extended to the case of partially sealed conditions, realized with the use of serrated piston rings [103]. The test results highlight the incidence of the lateral circumferential feeding groove on SFD behavior. The radial and tangential forces per unit length at the supply groove and at the bearing land were obtained, from integration of the circumferential pressure distributions, so as to test the effect of the groove depth (the values of 5 and 10 were given to the ratio between the groove depth and the radial clearance). The results from the tests showed that the forces per unit length at the groove were comparable to corresponding forces at the land, especially for the shallowest groove. The comparison of the radial forces, for uncavitated conditions, was particularly significant and underlined the role of the inertia effects in

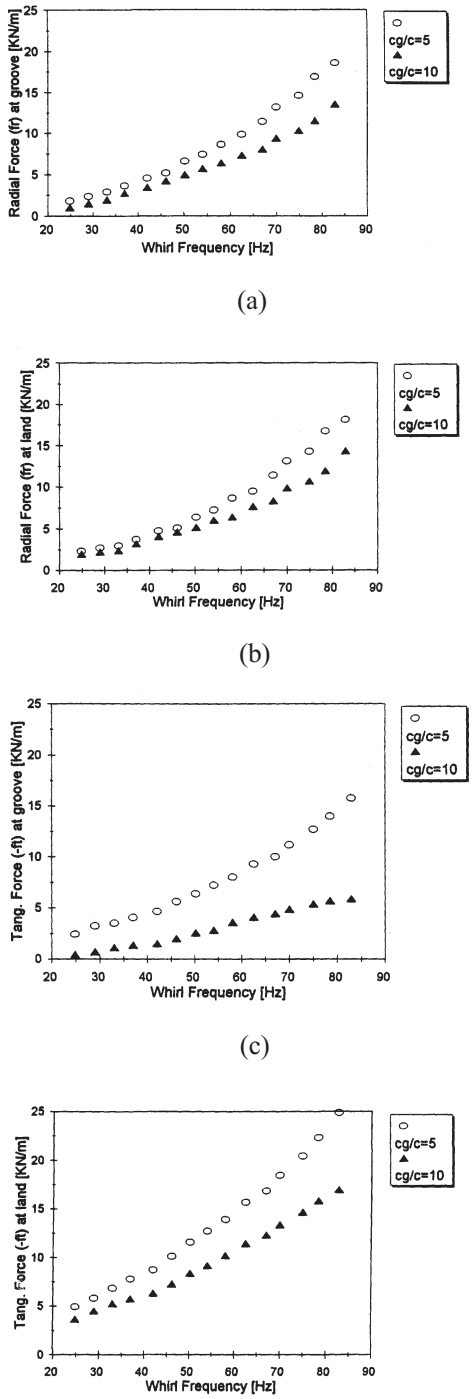

Figure 16. Film forces per unit axial length of the bearing, measured at the groove and at the land, versus the orbit frequency. Two values of the ratio between the groove depth *cg* and the radial clearance *c* at the lands were compared. (a) Radial force at the groove, (b) radial force at the land, (c) tangential force at the groove, (d) tangential force at the land (reproduced by permission of the ASME [103])

the groove (Figures 16(a), (b)). An appreciable contribution of the (shallowest) groove to the whole tangential force of the damper was also to be taken into account (Figures 16(c), (d)).

Rouch [54] evaluated the transfer function representing the complex ratio between the sinusoidal force applied to the damper and the resulting displacement (a linearized one degree of freedom model was realized), with a significant separation of the coefficient of the imaginary part (a damping coefficient) from the coefficient of the real part. The latter represented an *equivalent stiffness coefficient*, with a negative contribution of fluid inertia that became considerable when experimenting at high frequency with low viscosity oil. *Hydrodynamic stiffness* of the film was also observed by Roberts et al. [131] and Ellis et al. [84], who adopted an SFD provided with a central groove, in order to determine the linearized coefficients corresponding to assigned static equilibrium positions of the journal. They observed values of the damping action at a ratio from two to six with respect to the theoretical data, depending on the size of the groove. Inertia effects one order of magnitude higher than the theoretical predictions were also detected.

The experimental data reported by Zeidan and Vance [67] about the radial and tangential damping coefficients well illustrated the *inversion of the radial force* as a consequence of the opposing effects due to inertia and cavitation, when increasing the frequency of the journal precession. The direction of the radial force *changed from outward to inward* (*stiffening force effect*), as the result of changing from uncavitated film conditions, *dominated by the fluid inertia*, to conditions *dominated by the gaseous cavitation*. The effect of pressurization was also tested, showing that the gradual rise in the inlet pressure, at low to medium eccentricities, made the tangential force increase about linearly with the supply pressure, until it leveled off at a maximum value corresponding to the onset of full film conditions. The authors stress the fact that, before achieving uncavitated conditions, a *change from gaseous to vapor* regime of cavitation occurred.

This change was responsible for a *gradual inversion in the direction of the radial force*, *since the inertia forces turned out to dominate under conditions of vapor cavitation*, *unlike the gaseous regime that was characterized by a stiffening (inward) force*. This different influence of distinct cavitating conditions was negligible when the same test, with increase of the supply pressure, was repeated *at higher eccentricities*, *since the radial forces were stiffening in any case, regardless of the type of rupture* affecting the cavitated film.

Zhang et al. [107] carried out tests on a short, open-ended SFD, provided with a central groove for the oil supply. Different frequencies of journal precession and levels of pressurization were adopted. An algebraic extraction of the film force coefficients was achieved through measurement of the different radii of the CCOs resulting each time from the application of assigned external forces. The full-film operation, observed for eccentricities lower than about 0.5, involved the determination of only three coefficients, represented by a direct tangential damping coefficient, a direct radial inertia coefficient and a further direct radial stiffness coefficient, included in the analysis in accordance with the results from [84]. The determination of the coefficients for the cavitated regime proved less straightforward and was set aside. The experimental tangential and radial forces versus the journal eccentricity, for different values of the supply pressure, were plotted in Figures 17(a), (b). The diagrams

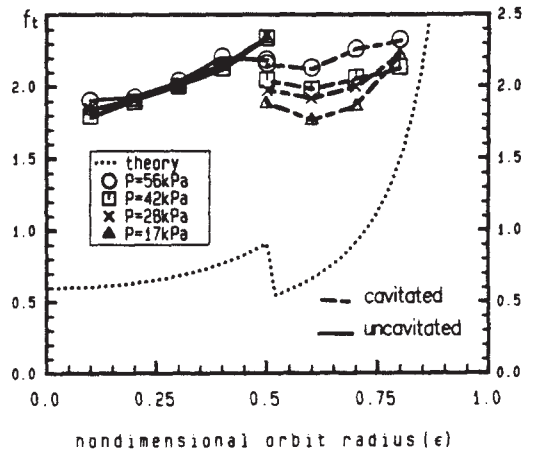

(a)

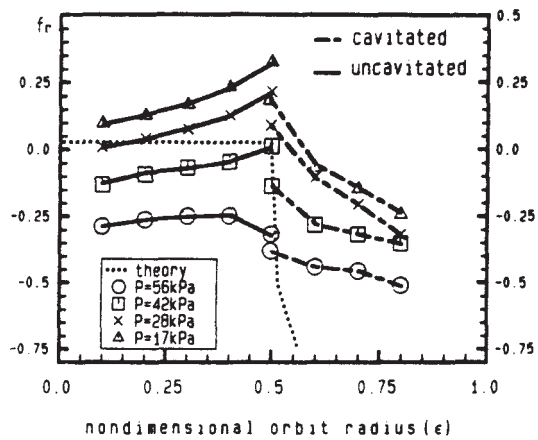

(b)

Figure 17. Influence of pressurization on the film forces measured on varying the orbit radius (fixed orbit frequency). (a) Tangential force versus orbit radius; (b) radial force versus orbit radius (reproduced by permission of the ASME [107])

show the relative irrelevance of the level of supply pressure on the tangential force until cavitation set in (Figure 17(a)) and an appreciable effect on the radial force (Figure 17(b)). The comparison of these data and the measured coefficients with the corresponding theoretical results from [36] was quite unsatisfactory in terms of both magnitude (tangential force and tangential coefficient) and qualitative trend (radial force and inertia coefficient; the measured inertia coefficient increased with the journal eccentricity, in any case, against the theoretical prediction from [36] or [41]). In this regard it is worth noting that the data compared were not completely congruent, since the stiffness effect assumed in the measured radial force was absent in the theoretical model. Furthermore, as remarked by the same authors, the role of important factors was ignored in the theoretical model. For instance, the difference in magnitudes of the tangential force and damping coefficients, from the experimental case to the theoretical one, was ascribed to a possible effect of the oil feed groove (as recognized in other studies like [85]).

Partially sealed conditions were investigated by Meng et al. [65] and Jung et al. [105]. In [65] the radial and tangential forces were measured, at a fixed orbit radius ($\varepsilon = 0.5$), and different testing conditions regarding the frequency of journal precession, the supply pressure and the oil temperature. It could be inferred that, in the presence of inertia effects, the influence of supply pressure, oil temperature and cavitation was more pronounced on the radial than tangential force (as in [107]). In [105] experimental values of the force coefficients were measured at different values of Re* (Re* up to 50 were obtained with adoption of three different lubricants). The reduction in the damping and inertia coefficients due to cavitation was experimentally confirmed (as in Figure 17 from [107]), even though the measured values appeared high when compared with the theoretical values, probably due to the substantial uniformity of the pressure in the axial direction affecting the laboratory model, owing to the partially sealed arrangement.

Diaz and San Andrés [126], in line with previous work [120–125] on cavitation owing to air entrainment in open-end SFDs (see Section 6.1), compared theoretical and experimental data with regard to the effect of the amount of air ingested by the SF (air volume fraction of the mixture – the flow was modeled as a mixture) on pressure distribution and film force. In practice, peak film pressure and tangential force exhibited a linear decrease with the air volume fraction. The radial force (due to cavitation) showed an increase for small values of the air volume fractions, an almost constant value for fractions of air up to about 80% and a decrease to zero for higher amounts of the entrained air. The crucial dependence of these effects on the oil flow rate and the whirl frequency that characterized the operation of the SFD was also characterized while testing the adequacy of the theoretical model. Investigation of this matter will probably be continued in future work.

7. Conclusions of Part I

The theoretical and experimental characterization of the SFD, as a whole component, was the aim pursued by the research work reviewed in Part I of this paper.

Determination of appropriate expressions for the fluid film force and the related coefficients represented the main goal shared by the investigations referred above. The review pointed out the attention paid by researchers to factors capable of considerably influencing SFD response. Besides the geometrical parameters of the damper, the way oil is supplied to the SF, the presence and the type of seals, the fluid inertia and the cavitation in the film deserve particular interest.

The theoretical refinements of the basic theory and the connected experimental work were generally carried out within models that were characterized by assigned relative motions between the *journal* and the *bearing* of the damper. Motions of the journal represented by circular centered orbits (CCOs) or small orbits about a position eccentric respect to the bearing center were largely adopted.

The following Part II [4] of the review is addressed to research work on the rotordynamic evaluation of the SFD, i.e. the characterization of the role of the SFD in the dynamic behavior of rotors on supports equipped with such dampers. State-of-the-art research and the trends of future investigation in the area are the focus of the concluding section of [4].

References

[1] Cooper, S., 1963, "Preliminary Investigation of Oil Films for Control of Vibration", *Proc. Lubrication and Wear Convention, Inst. Mech. Engin.*, 305–315.

[2] Friedericy, J. A., Eppink, R. T., Liu, Y. N., and Cetiner, A., 1965, "An Investigation of the Behavoiur of Floating Ring Dampers and the Dynamics of Hypercritical Shaft on Flexible Supports," *USAAML Technical Report 65-34, UVA Report No. CE-33440-104-65U*.

[3] Zeidan, F., San Andrés L. A., and Vance, J. M., 1996, "Design and Application of Squeeze Film Dampers in Rotating Machinery," *Proceedings of the Twenty-Fifth Turbomachinery Symposium*, *Turbomachinery Laboratory, Texas A&M University, College Station, TX*, 169–188.

[4] Adiletta, G., and Della Pietra, L., 2002, "The Squeeze Film Damper over Four Decades of Investigations. Part II: Rotordynamic Analyses with Rigid and Flexible Rotors," *The Shock and Vibration Digest*, to be published.

[5] Hamburg, G., and Parkinson, J., 1962, "Gas Turbine Shaft Dynamics," *SAE Transactions*, Vol. 70, 774–784.

[6] Birmann, R., 1933, US Patent 1,926,225, "Turbo Compressor".

[7] Birmann, R., 1946, US Patent 2,403,489, "Bearing Construction for Turbines or the like".

[8] Birmann, R., 1948, US Patent 2,440,890, "Turbine Bearing".

[9] Hahn, E. J., and Simandiri, S., 1974, "Squeeze Film Mounts for Vibration Attenuation in Rigid Rotors," *Proc. Noise, Shock & Vibration Conference*, Monash Univ., Melbourne.

[10] Glienicke, J., and Stanski, U., 1975, "External Bearing Damping, a Mean of Preventing Dangerous Shaft Vibrations on Gas Turbines and Exaust Turbo-Chargers," *CIMAC 11th Int. Congress on Combustion Engines*, Barcelona, 287–311.

[11] Magge, N., 1975, "Philosophy, Design and Evaluation of Soft-Mounted Engine Rotor Systems," *J. Aircraft*, Vol. 12, 4, 318–324.

[12] Malanowski, S., 1979, "Case Histories in which Subsynchronous or Synchronous Vibration Amplitudes have been Minimized after Employing Custom Designed Damper Bearings," *Proceedings of the Conference on the Stability and Dynamic Response of Rotors with Squeeze-Film Bearings, University of Virginia.*

[13] Arauz, G. L., and San Andrés, L. A., 1993, "Experimental Pressures and Film Forces in a Squeeze Film Damper," *ASME J. Tribology*, Vol. 115, 134–140.

[14] Kanki, H., Kaneko, Y., Kurosawa, M., and Yamamoto, T., 1998, "Prevention of Low-Frequency Vibration of High-Capacity Steam Turbine Units by Squeeze-Film Damper," *ASME J. Engineering for Gas Turbines and Power*, Vol. 120, 391–396.

[15] Cookson, R. A., and Kossa, S. S., 1981, "The Vibration Isolating Properties of Uncentralized Squeeze-Film Damper Bearings Supporting a Flexible Rotor," *ASME J. Engineering for Power*, Vol. 103, 781–787.

[16] Gunter, E. J., and Allaire, P. E., 1976, "Stabilization of Turbomachinery with Squeeze Film Dampers – Theory and Applications," *IMechE, C233/76*, 291–300.

[17] Vance, J. M., 1988, *Rotordynamics of Turbomachinery*, Wiley & Sons, New York.

[18] Zeidan, F., 1995, "Application of Squeeze Film Dampers," *Turbomachinery International*, Vol. 112, 50–53.

[19] Zhao, J. Y., and Hahn, E. J., 1995, "Eccentric Operation and Blade-Loss Simulation of a Rigid Rotor Supported by an Improved Squeeze Film Damper," *ASME J. Tribology*, Vol. 117, 490–497.

[20] de Santiago, O., San Andrés, L., and Oliveras, J., 1999, "Imbalance Response of a Rotor Supported on Open-Ends Integral Squeeze Film Dampers," *ASME J. Engineering for Gas Turbines and Power*, Vol. 121, 718–721.

[21] Zhang, S. P., Yan, L. T., and Li, Q. H., 1993, "The Effectiveness of Porous Squeeze Film Dampers for Suppressing Nonsynchronous Motions," *ASME J. Vibration and Acoustics*, Vol. 115, 16–18.

[22] El-Shafei, A., 1993, "Experimental and Analytical Investigation of Hybrid Squeeze Film Dampers," *ASME J. Engineering for Gas Turbines and Power*, Vol. 115, 353–359.

[23] Suciu, C. V., Bonneau, O., Brun-Picard, D., Frêne, J., and Pascovici, M. D., 2000, "Study of a Novel Squeeze Film Damper and Vibration Generator, *ASME J. Tribology*, Vol. 122, 211–218.

[24] Holmes, R., 1990, "The Control of Rotor Vibration Using Squeeze Film Dampers," *Vibration and Wear in High Speed Rotating Machinery*, J. M. Montalvao e Silva, and F. A. Pina da Silva, eds., Kluwer Academic Publishers, Dordrecht, 399–412.

[25] Cunningham, R. E., 1978, "Steady-State Unbalance Response of a Three-Disk Flexible Rotor on Flexible, Damped Supports" *ASME J. Mechanical Design*, Vol. 100, 563–573.

[26] Memmott, E. A., 1992, "Stability of Centrifugal Compressors by Applications of Tilt Pad Seals, Damper Bearings and Shunt Holes," *Proceedings, 5th International Conference on Vibrations in Rotating Machinery, ImechE, C432/070*, 99–106.

[27] Memmott, E. A., 1999, "Stability Analysis and Testing of a Train of Centrifugal Compressors for High Pressure Gas Injection," *ASME J. Engineering for Gas Turbines and Power*, Vol. 121, 509-514.

[28] Powell, J. W., and Tempest, M. C., 1968, "A Study of High Speed Machines with Rubber Stabilized Air Bearings," *ASME Paper, No. 68-LubS-9, J. Lubrication Technology*, 701–708.

[29] Smalley, A. J., Darlow, M. S., and Metha, R. K., 1978, "The Dynamic Characteristics of O'-Rings," *ASME Paper, No. 77-DET-27, J. Mechanical Design*, Vol. 100, 132–146.

[30] Tecza, J. A., Darlow, M. S., Jones, S., Smalley, A., and Cunningham, R., 1979, "Elastometer mounted rotors – An alternative for smoother running turbomachinery," *ASME paper, No. 79-GT-149, Gas Turbine Conference*, San Diego, CA.

[31] Tecza, J. A., Smalley, A., Darlow, M. S., and Cunningham, R., 1979, "Design of elastometer damper for high-speed flexible rotors," *ASME paper, No. 79-DET-98, Design Engineering Technical Conference*, St. Louis, MO.

[32] Darlow, M., and Zorzi, E., 1981, *Mechanical Design Handbook for Elastomers*, Mechanical Technology Inc. , Latham, NY.

[33] Holmes, R., and Dogan, M., 1985, "The Performance of a Sealed Squeeze Film Bearings in a Flexible Support Structure," *ImechE, Proc. Inst. Mech. Engrs.*, Vol. 199, N. C1, 1–9.

[34] White, D. C., 1970, "Squeeze Film Journal Bearings," Ph.D. Dissertation, Cambridge University.

[35] El-Shafei, A., and Crandall, S. H., 1991, "Fluid Inertia Forces in Squeeze Film Dampers," *ASME, Rotating Machinery and Vehicle Dynamics, DE-35*, 219-228.

[36] Zhang, J., Ellis, J., and Roberts, J. B., 1993, "Observations on the Non Linear Fluid Forces in Short Cylindrical Squeeze Film Dampers," *ASME J. Tribology*, Vol. 115, 692–698.

[37] Szeri, A. Z., Raimondi, A. A., and Giron-Duarte A., 1983, "Linear Force Coefficients for Squeeze Film Dampers," *ASME J. Lubrication Technology*, Vol. 105, 326–334.

[38] Tichy, J. A., 1983, "The effect of Fluid Inertia in Squeeze Film Damper Bearings: a Heuristic and Phisical Description," *ASME paper, No. 83-GT-177*.

[39] Hahn, E. J., 1979, "Stability and Unbalance Response of Centrally Preloaded Rotors Mounted in Journal and Squeeze Film Bearings," *ASME J. Lubrication Technology*, Vol. 101, 120–128.

[40] Holmes, R., and Sykes, J. E. H., 1989, "Large-Amplitude Vibrations in Rotor Assemblies," *J. Sound and Vibration*, Vol. 133(2), 337–351.

[41] San Andrés, L. A., and Vance, J. M., 1986, "Effects of Fluid Inertia and Turbulence on the Force Coefficients for Squeeze Film Dampers," *ASME J. Engineering for Gas Turbines and Power*, Vol. 108, 332–339.

[42] Booker, J. F., 1965, "Dinamically Loaded Journal Bearings: Mobility Method of Solution," *ASME J. Basic Engineering*, September, 537–546.

[43] Muskat, M., and Morgan, F., 1938, "Studies in Lubrication. I. The Theory of Thick Film Lubrication of a Complete Journal Bearing of Finite Length," *J. Applied Physics*, Vol. 9, 393.

[44] El-Shafei, A., and Eranki, R. V., 1992, "Dynamic Force Coefficients of Short and Long Squeeze Film Dampers Executing Elliptic Orbits," *Proceedings, 5th International Conference on Vibrations in Rotating Machinery, ImechE, C432/127*, 597–604.

[45] Dede, M. M., Dogan, M., and Holmes, R., 1985, "The Damping Capacity of a Sealed Squeeze Film Bearing," *ASME J. Tribology*, Vol. 107, 411–418.

[46] Feder, E., Bansal, P. N., and Blanco, A., 1978, "Investigation of Squeeze Film Damper Forces produced by Circular Centered Orbits," *ASME J. Engineering for Power*, Vol. 100, 15–21.

[47] Bansal, P. N., and Hibner, D. H., 1978, "Experimental and Analytical Investigation of Squeeze Film Bearing Damper Forces induced by Offset Circular Whirl Orbits," *ASME J. Mechanical Design*, Vol. 100, 549–557.

[48] Vance, J. M., and Kirton, A. J., 1975, "Experimental Measurement of the Dynamic Force Response of a Squeeze-Film Bearing Damper," *ASME J. Engineering for Industry*, Nov., 1282–1290.

[49] Lund, J. W., Smalley, A. J., Tecza, J. A., and Walton, J. F., 1983, "Squeeze Film Damper Technology: Part 1 – Prediction of Finite Length Damper Performance," *ASME paper*, *No. 83-GT-247*.

[50] Marmol, R. A., and Vance, J. M., 1978, "Squeeze Film Damper Characteristics for Gas Turbine Engine," *ASME J. Mechanical Design*, Vol. 100, 139–146.

[51] Tichy, J. A., 1987, "A Study of the Effect of Fluid Inertia and End Leakage in the Finite Squeeze Film Damper," *ASME J. Tribology*, Vol. 109, 54–59.

[52] Tecza, J. A., Giordano, J. C., Zorzi, E. S., and Drake, S. K., 1983, "Squeeze Film Damper Technology: Part 2 – Experimental Verification Using a Controlled-Orbit Test Rig," *ASME paper, No. 83-GT-248*.

[53] Miyachi, T., Hoshiya, S., Matsuki, Y., and Torisaki, T., 1979, "Oil Squeeze Film dampers for Reducing Vibration of Aircraft Turbine Engines," *ASME paper 79-GT-133*.

[54] Rouch, K. E., 1990, "Experimental Evaluation of Squeeze Film Damper Coefficients with Frequency Domain Techniques," *STLE Tribology Transactions*, Vol. 33, number 1, 67–75.

[55] San Andrés, L., and Lubell, D., 1998, "Imbalance Response of a Test Rotor Supported on Squeeze Film Dampers," *ASME J. Engineering for Gas Turbines and Power*, Vol. 120, 397–404.

[56] Chen, P.Y.P., and Hahn, E. J., 2000, "Side clearance effects on squeeze film damper performance," *Tribology International*, Vol. 33, 161–165.

[57] San Andrés L. A., and Vance, J. M., 1987, "Effects of Fluid Inertia on Finite-Length Squeeze Film Dampers," *ASLE Transactions*, Vol. 30, number 3, 384–393.

[58] Arauz, G. L., and San Andrés, L. A., 1994, "Effect of a Circumferential Feeding Groove on the Dynamic Force Response of a Short Squeeze Film Damper," *ASME J. Tribology*, Vol. 116, 369–377.

[59] Ramli, M. D., Roberts, J. B., and Ellis, J., 1987, "Determination of Squeeze Film Dynamic Coefficients from Experimental Transient Data," *ASME J. Tribology*, Vol. 109, 155–163.

[60] San Andrés, L. A., 1985, "Effect of Fluid Inertia on Squeeze Film Damper Force Response," Ph.D. thesis, Texas A&M University.

[61] San Andrés L. A., and Vance, J. M., 1987, "Experimental Measurement of the Dynamic Pressure Distribution in a Squeeze-Film Bearing Damper Executing Circular-Centered Orbit," *ASLE Transactions*, Vol. 30, No. 3, 373–383.

[62] Walton II, J. F, Walovit, J. A., Zorzi, E. S., and Schrand, J., 1987, "Experimental Observation of Cavitating Squeeze-Film Dampers," *ASME J. Tribology*, Vol. 109, 290–295.

[63] San Andrés, L. A., 1992, "Analysis of Short Squeeze Film Dampers with a Central Groove," *ASME J. Tribology*, Vol. 114, 659–665.

[64] Chen, P.Y.P., and Hahn, E. J., 1994, "Pressure Distribution in Squeeze Film Dampers with Oil Hole Feed," ImechE, Proc. Inst. Mech. Engrs., *J. Engineering Tribology*, Vol. 208, 105–112.

[65] Meng, G., San Andrés, L. A., and Vance, J. M., 1991, "Experimental Investigation on the Dynamic Pressure and Force Response of a Partially Sealed Squeeze Film Damper," *ASME Rotating Machinery and Vehicle Dynamics*, DE-Vol. 35, 251–256.

[66] Zeidan, F., and Vance, J., 1989, "Cavitation leading to a Two Phase Fluid in a Squeeze Film Damper," *STLE Tribology Transactions*, Vol. 32, No. 1, 100–104.

[67] Zeidan, F., and Vance, J., 1989, "Experimental Investigation of Cavitation Effects on the Squeeze Film Force Coefficients," *Proceedings of the 12th Biennial ASME Conference on Mechanical Vibration and Noise*, Montreal, Canada, DE - 18-1, 237–242.

[68] Ku, C.-P., and Tichy, J. A., 1990, "An Experimental and Theoretical Study of Cavitation in a Finite Submerged Squeeze Film Dampers," *ASME J. Tribology*, Vol. 112, 725–733.

[69] Simandiri, S., and Hahn, E. J., 1976, "Effect of Pressurization on the Vibration Isolation Capability of Squeeze Film Bearings," *J. Engineering for Industry*, Vol. 98, Series B, No. 1, 109–117.

[70] Booker, J. F., 1965, "A Table of the Journal-Bearing Integral," *ASME J. Basic Engineering*, June, 533–535.

[71] Williams, R. J., and Holmes, R., 1971, "Determination of the Linear Characteristics of Squeeze Film," *Instn. Mech. Engrs.*, C81/71, 135–141.

[72] San Andrés L. A., and Vance J. M., 1988, "Effects of Fluid Inertia on the Performance of Squeeze-Film Damper Supported Rotors," *J. Engineering for Gas Turbines and Power*, Vol. 110, 51–57.

[73] Kinsale, J. C., 1989, "Numerical and Experimental Study of a Finite Submerged Squeeze Film Damper," Ph. D. Thesis, Rensselaer Polytechnic Institute, Troy, N.Y..

[74] Modest, M. F., and Tichy, J. A., 1978, "Squeeze Film Flow in Arbitrarily Shaped Journal Bearings Subject to Oscillations," *ASME J. Lubrication Technology*, Vol. 100, 323–329.

[75] Ramli, M. D., Ellis, J., and Roberts, J. B., 1987, "On the Computation of Inertial Coefficients in Squeeze Film Bearings," ImechE, *Proc. Inst. Mech. Engrs.*, Vol. 201, No. C2, 125–131.

[76] San Andrés L. A., 1988, "Effects of Fluid Inertia on Force Coefficients for the Long Squeeze-Film Damper," *STLE Tribology Transactions*, Vol. 31, No. 3, 370–375.

[77] San Andrés L. A., and Vance, J. M., 1987, "Effects of Fluid Inertia on Squeeze-Film Damper Forces for Small Amplitude Circular Centered Motions," *ASLE Transactions*, Vol. 30, No. 1, 63–68.

[78] San Andrés L. A., and Vance, J. M., 1987, "Force Coefficients for Open-Ended Squeeze-Film Dampers Executing Small-Amplitude Motions About an Off-Center Equilibrium Position," *ASLE Transactions*, Vol. 30, No. 1, 69–76.

[79] Tichy, J. A., and Winer, W., 1970, "Inertial Consideration in Parallel Circular Squeeze-Film Bearings," *ASME J. Lubrication Technology*, Vol. 92, 588–592.

[80] Tichy, J. A., 1982, "Effects of Fluid Inertia and Viscoelasticity on Squeeze Film Bearing Forces," *ASLE Transactions*, Vol. 25, No. 1, 125–132.

[81] Tichy, J. A., 1984, "Effects of Fluid Inertia and Viscoelasticity on the One Dimensional Squeeze Film Bearing," *ASLE Transactions*, Vol. 27, No. 2, 164–167.

[82] Tichy, J. A., and Bou-Saïd, B., 1991, "Hydrodynamic Lubrication and Bearing Behaviour with Impulsive Loads," *STLE Tribology Transactions*, Vol. 34, No. 4, 505–512.

[83] Ellis, J., Roberts, J. B., and Hosseini Sianaki, A., 1988, "A Comparison of Identification Methods for Estimating Squeeze Film Damper Coefficients," *ASME J. Tribology*, Vol. 110, 119–127.

[84] Ellis, J., Roberts, J. B., and Ramli, M. D., 1989, "The Experimental Determination of Squeeze-Film Dynamic Coefficients Using the State Variable Filter Method of Parametric Identification," *ASME J. Tribology*, Vol. 111, 252–259.

[85] Ellis, J., Roberts, J. B., and Hosseini Sianaki, A., 1990, "The Complete Determination of Squeeze Film Linear Dynamic Coefficients from Experimental Data," *ASME J. Tribology*, Vol. 112, 712–724.

[86] Roberts J. B., Holmes R., and Mason P. J., 1986, "Estimation of Squeeze-Film Damping and Inertial Coefficients from Experimental Free-Decay Data," ImechE, *Proc. Instn. Mech. Engrs*., Vol. 200, No. C2, 123–133.

[87] Roberts, J. B., Ellis, J., and Hosseini Sianaki, A., 1990, "The Determination of Squeeze Film Dynamic Coefficients from Transient Two-Dimensional Experimental Data," *ASME J. Tribology*, Vol. 112, 288–298.

[88] San Andrés L. A., Meng G., and Yoon S., 1993, "Dynamic Force Response of an Open-Ended Squeeze Film Damper," *ASME J. Engineering for Gas Turbines and Power*, Vol. 115, 341–346.

[89] Simandiri, S., and Hahn, E. J., 1979, "Experimental Evaluation of the Predicted Behaviour of Squeeze Film Bearing Supported Rigid Rotors," ImechE, *J. Mechanical Engineering Science*, Vol. 21, No. 6, 439–451.

[90] Tichy, J. A., 1986, "The Effect of Fluid Inertia in Hydrodynamic Lubrication Studied by a Linearization Method: Two Useful Applications," *International J. Engineering Science*, Vol. 24, 10, 1607–1613.

[91] Crandall, S. H., and El-Shafei, A., 1993, "Momentum and Energy Approximations for Elementary Squeeze Film Damper Flows, *ASME J. Applied Mechanics*, Vol. 60, 728–736.

[92] Pinkus, O., and Sternlicht, B., 1961, *Theory of Hydrodynamic Lubrication*, McGraw-Hill Book Co., N.Y.

[93] Costantinescu, V. N., 1970, "On the Influence of Inertia Forces in Turbulent and Laminar Self-Acting Films," *ASME J. Lubrication Technology*, Vol. 92, 473–479.

[94] Reinhardt, E., and Lund, J. W., 1975, "The Influence of Fluid Inertia on the Dynamic Properties of Journal Bearings," *ASME J. Lubrication Technology*, Vol. 97, 159–167.

[95] Smith, D. M., 1965, "Journal Bearing Dynamic Characteristics-Effect of Inertia Lubricant," *Proc. Instn. Mech. Engrs*., Vol. 179, Pt.3J, 37–44.

[96] Tichy, J. A., 1978, "The Behaviour of Viscoelastic Squeeze Films Subject to Normal Oscillations, Including the Effect of Fluid Inertia," *Applied Scientific Research*, 33, 501–517.

[97] Tichy, J. A., and Modest, M. F., 1978, "Squeeze Film Flow between Arbitrary Two-Dimensional Surfaces Subject to Normal Oscillations," *ASME J. Lubrication Technology*, Vol. 100, 316–322.

[98] Tichy, J. A., and Skinkle, M. E., 1979, "An Analysis of the Flow of a Viscoelastic Fluid between Arbitrary Two-Dimensional Surfaces

Subject to High Frequency Normal Oscillations," *ASME J. Lubrication Technology*, Vol. 101, 145–153.

[99] Modest, M. F., and Tichy, J. A., 1979 "The Slider Bearing with Small Superimposed Normal Oscillation, Including the Effect of Fluid Inertia," *ASLE Transactions*, Vol. 22, 4, 358–360.

[100] Warner, P. C., 1963, "Static and Dynamic Properties of Partial Journal Bearings," *ASME J. Basic Engineering*, June, 247–257.

[101] Tichy, J. A., and Bourgin, P., 1985, "The Effect of Inertia in Lubrication Flow Including Entrance and Initial Conditions," *ASME J. Applied Mechanics*, Vol. 52, 752–765.

[102] San Andrés, L., 1986, "Experimental Results for SFD TRC Test Rig with a Serrated Piston Ring," Internal Report, May, *Turbomachinery Research Consortium*, Texas A&M University.

[103] Arauz, G. L., and San Andrés, L. A., 1996, "Experimental Study on the Effect of a Circumferential Feeding Groove on the Dynamic Force Response of a Sealed Squeeze Film Damper," *ASME J. Tribology*, Vol. 118, 900–905.

[104] Jung, S. Y., San Andrés, L. A., and Vance, J. M., 1991, "Measurements of Pressure Distributions and Force Coefficients in a Squeeze Film Damper Part I: Fully Open Ended Configuration," *STLE Tribology Transactions*, Vol. 34, 3, 375–382.

[105] Jung, S. Y., San Andrés, L. A., and Vance, J. M., 1991, "Measurements of Pressure Distributions and Force Coefficients in a Squeeze Film Damper Part II: Partially Sealed Configuration," *STLE Tribology transactions*, Vol. 34, 3, 383–388.

[106] Tichy, J. A., 1984, "Measurement of Squeeze Film Bearing Forces to Demonstrate the Effect of Fluid Inertia," *ASME paper, No. 84-GT-11*.

[107] Zhang, J. J., Roberts, J. B., and Ellis, J., 1994, "Experimental Behaviour of a Short Squeeze Film Damper Executing Circular Centered Orbits," *ASME J. Tribology*, Vol. 116, 528–534.

[108] Della Pietra, L., 2000, "Analytical and Experimental Investigation of Squeeze-Film Dampers Executing Circular Orbits," *Meccanica*, Vol. 35, 2, 133–157.

[109] Tichy, J. A., 1985, "Measurement of Squeeze Film Bearing Forces and Pressures, Including the Effect of Fluid Inertia," *ASLE Transactions*, Vol. 28, No. 4, 520–526.

[110] Cole, J. A., and Hughes, C.J., 1956, "Oil Flow and Film Extent in Complete Journal Bearings," *Proc. Inst. Mech. Eng*., Vol. 170, 499–510.

[111] Cole, J. A., and Hughes, C. J., 1957, "Visual Study of Film Extent in Dynamically Loaded Complete Journal Bearings," *Proc. Instn. Mech. Engrs., Lubrication and Wear Conference*, paper 87, 147–150.

[112] Jakobsson, B., and Floberg, L., 1957, "The Finite Journal Bearing Considering Vaporization," Transactions Chalmers University of Technology, No. 190, Gothenburg, Sweden.

[113] Olsson, K.-O., 1965, "Cavitation in Dynamically Loaded Bearings," Transactions Chalmers University of Technology, No. 308, Gothenburg, Sweden.

[114] Dyer, D., and Reason, B. R., 1976, "A Study of Tensile Stresses in Journal-Bearing Oil Film," ImechE, *J. Mechanical Engineering Science*, Vol. 18, No. 1, 46–52.

[115] Jacobson, B. O., and Hamrock, B. J., 1983, "High-Speed Motion-Picture Camera Experiments of Cavitation in Dynamically Loaded Journal Bearings," *ASME J. Lubrication Technology*, Vol. 105, 446–452.

[116] Sun, D. C., Brewe, D. E., and Abel, P. B., 1993, "Simultaneous Pressure Measurement and Highspeed Photography Study of Cavitation in a Dynamically Loaded Journal Bearing," *ASME J. Tribology*, Vol. 115, No. 3, 88–95.

[117] Paydas, A., 1988, "An Investigation into Fluid Film Lubrication in Dynamically Loaded Bearings," PhD Thesis, Lancashire Polytechnic, U.K..

[118] Zeidan, F., and Vance, J., 1990, "Cavitation Regimes in Squeeze Film Dampers and their Effect on the Pressure Distribution," *STLE Tribology Transactions*, Vol. 33, No. 3, 447–453.

[119] Zeidan, F., and Vance, J., 1990, "Cavitation and Air Entrainment Effects on the Response of Squeeze Film Supported Rotors," *ASME J. Tribology*, Vol. 112, 347–353.

[120] Diaz, S. E., and San Andrés, L. A , 1998, "Measurement of Pressure in a Squeeze Film Damper with an Air/Oil Bubbly Mixture," *STLE Trib.Trans*., Vol. 41, 282–288.

[121] Diaz, S. E., and San Andrés, L. A , 1999, "Reduction of the Dynamic Load Capacity in a Squeeze Film Damper Operating with a Bubbly Lubricant," *ASME J. Engineering for Gas Turbines and Power*, Vol. 121, 703–709.

[122] Diaz, S. E., 1999, "The Effect of Air Entrapment on the Performance of Squeeze Film Dampers: Experiments and Analysis," Ph.D. Dissertation, Texas A&M University, College Station, TX.

[123] Nikolajsen, J. L., 1999, "Viscosity and Density Models for Aerated Oil in Fluid-Film Bearings," *STLE Trib. Trans*., Vol. 42, 186–191.

[124] Tao, L., Diaz, S. E., San Andrés, L. A , and Rajagopal, K. R., 2000, "Analysis of Squeeze Film Dampers Operating With Bubbly Lubricants," *ASME J. Tribology*, Vol. 122, 205–210.

[125] Beets, T., Diaz, S. E., and San Andrés, L. A., 2000, "Pressure Measurement and Flow Visualization of a SFD Operating With a Bubbly Lubricant," *Proceedings of the 2000 NSF Design and Manufacturing Researche Conference*, CD-rom, Vancouver, Canada.

[126] Diaz, S., and San Andrés, L. A , 2001, "A Model for Squeeze Film Dampers Operating with Air Entrainment and Validation With Experiments," *ASME J. Tribology*, Vol. 123, 125–133.

[127] Humes, B., and Holmes, R., 1978, "The Role of Sub-Atmospheric Film Pressures in the Vibration Performances of Squeeze Film Bearings," ImechE, *J. Mechanical Engineering Science*, Vol. 20, No. 5, 283–289.

[128] Holmes, R., and Dede, M. M., 1980, "Dynamic Pressure Determinations in a Squeeze Film Damper," ImechE, *Proc. Inst. Mech. Engrs*., C260/80, 71–75.

[129] Zhao, J. Y., Linnet, I. W., and McLean, L. J., 1998, "Unbalance Response of a Flexible Rotor Supported by a Squeeze Film Damper," *ASME J. Vibration and Acoustics*, Vol. 120, 32–38.

[130] Feng, N. S., and Hahn, E. J., 1987, "Effects of Gas Entrainment on Squeeze Film Damper Performance," *ASME J. Tribology Transactions*, Vol. 109, 149–154.

[131] Roberts, J. B., Ramli, M. D., and Ellis, J., 1988, "Experimental Determination of Squeeze-Film Damping Coefficients by a Frequency Domain Method," IMechE, *Proc. Instn. Mech. Engrs*., Vol. 202, No. C4, 235–244.